ENERGYSOLUTIONS

October 10, 2023

CD-2023-199

Mr. Doug Hansen, Director
Utah Division of Waste Management and Radiation Control
195 North 1950 West
Salt Lake City, Utah 84114-4880

Re: Responses to Federal Cell Facility Application Request for Information - DRC-2023-000537

Dear Mr. Hansen:

EnergySolutions hereby responds to the Utah Division of Waste Management and Radiation Control's January 19, 2023 Request for Information (RFI) on our Federal Cell Facility Application.[1] A response is provided for each request using the Director's assigned reference number.

Appendix O: Unsaturated Zone Modeling

▪ ***O-9***

Unsaturated Zone Scaling- Well documented procedures consistent with current practice are necessary to define input parameters that are representative of spatially averaged conditions, and the uncertainty in these spatial averages. No basis consistent with existing practice has been provided for the scaling approach used in the Clive DU PA v2.0, where central tendencies for hydraulic properties are represented by arithmetic or geometric means and uncertainty is described by the standard error from historical databases. The standard error of the mean has been proffered to account for uncertainty, but the appropriateness of the standard error has not been demonstrated as an accepted method in hydrologic practice. Please provide a quantitative assessment consistent with accepted hydrologic practice that demonstrates the validity of the scaling approach used in Clive DU PA v2.0.

Scaling approaches applied for the DU PA are consistent with accepted hydrologic practice as discussed below. A challenge with the development of any Performance Assessment (PA) model is accurately representing real world conditions in the model inputs. PA models represent processes with varying intrinsic temporal and spatial scales, covering large spaces (volumes or areas) and times (thousands of years). Available data typically do not correspond to the spatial

[1] Hansen, D.J. "Federal Cell Facility Application Request for Information." via DRC-2023-000525 from the Utah Division of Waste Management and Radiation Control to Vern Rogers of Energy*Solutions*, January 19, 2023.

and temporal resolution of a PA model.[2] Data gleaned from literature reviews often correspond to specific points in time and space and, as such, characterize variability associated with the underlying populations rather than variability associated with much larger spaces and time frames. Hence, for complex probabilistic models such as PA models, scaling is undertaken to rectify spatial and temporal scale differences between processes, observations, and models. For probabilistic modeling appropriate scaling is essential, as has been acknowledged in many references obtainable from the hydrologic modeling literature, climate change modeling literature, and any other modeling domains for which the spatial and temporal scales of the data are different than those of the models. Scaling must be done carefully so that risk dilution is not a result. Hydrologic and PA modeling tends to use upscaling for both spatial and temporal domains, because available data often tend to represent essentially points in space and time (or very small volumes and time frames compared to the model domains), whereas climate change modeling tends to involve downscaling spatially and upscaling temporally, because the available spatial data represent larger areas/volumes than needed to understand important localized effects of climate change.

Spatial and temporal scaling are important considerations in groundwater modeling. Groundwater systems exhibit spatial heterogeneity and temporal variability, which necessitate appropriate scaling techniques for accurate representation and prediction of groundwater flow and contaminant transport processes. References that discuss the need for spatial and temporal scaling in groundwater modeling include:

1. Anderson et al. (2015). This book provides an in-depth discussion of groundwater modeling techniques, including the consideration of spatial and temporal scaling in simulating flow and advective transport processes.
2. Dagan (1989). This book presents a theoretical approach to understanding flow and transport in porous formations, highlighting the importance of appropriate scaling for accurate modeling of these processes.
3. Therrien and Sudicky (1996). This paper discusses the use of three-dimensional numerical models for variably saturated flow and contaminant transport, emphasizing the need for proper spatial scaling to capture heterogeneity in subsurface properties.
4. Tillman et al. (2018). This paper argues that coarser spatial and longer temporal scale climate data may be sufficient for simulating changes in groundwater recharge, particularly for providing water resources managers an understanding of trends in recharge over water year or longer time scales.

[2] For example, the raw biotic data essentially represent points in time and space; they do not represent the spatial scale of the model, which is a large area. The precipitation data represent points in time and space, but the model has a time domain ranging from several years (time steps) to 10,000 years (compliance period) or longer. The hydrological data from the test cell represent points in time and space over its roughly 20-year service life, but the model has a time domain of thousands of years, and a spatial domain of the much larger waste cell.

These references cover various aspects of groundwater modeling and highlight the significance of spatial and temporal scaling in capturing the complexity and dynamics of groundwater flow and contaminant transport.

Infiltration modeling is another crucial aspect of hydrologic modeling that focuses on the process of water entering the soil surface. Spatial and temporal scaling considerations play an important role in accurately simulating infiltration processes. References that discuss the need for spatial and temporal scaling in infiltration modeling include:

1. Smith et al. (2002). This comprehensive monograph provides an in-depth discussion on infiltration theory, including spatial and temporal scaling considerations for modeling infiltration processes.
2. Beven and Germann (1982). This paper discusses the role of macropores in infiltration processes and the challenges associated with scaling from laboratory-scale experiments to field-scale applications.
3. Chari et al. (2020). This paper describes a new scaling method for prediction of infiltration spatial variations. Instead of using infiltration equation parameters, the amount of water infiltrated into the soil at a given time is used to obtain the infiltration equation scaling factor.

These references provide insights into the importance of spatial and temporal scaling in infiltration modeling. They explore the challenges, scaling relationships, and approaches for accurately representing infiltration processes at different scales.

Spatial scaling for climate change modeling often involves downscaling instead of upscaling. Otherwise, the basic principles of scaling still apply. The goal of both spatial and temporal scaling in climate change modeling is to provide more detailed and localized climate information that is relevant for assessing the impacts of climate change on specific regions, ecosystems, and human systems. These scaled-down data are crucial for making informed decisions and planning effective adaptation strategies. References that delve into the topic of spatial and temporal scaling in climate change modeling include:

1. Wilby and Wigley (1997)
2. Fowler et al. (2007)
3. Maraun et al. (2010)
4. Maraun (2013)
5. Diffenbaugh and Giorgi (2012)
6. Christensen et al. (1996)
7. Rummukainen (2010)
8. Wuebbles and Hayhoe (2004)
9. Teutschbein and Siebert (2012)
10. Maraun et al. (2017)

These references cover a range of topics related to spatial and temporal scaling in climate change modeling, including downscaling techniques, regional climate models, bias correction methods, and the application of scaled climate data for impact assessments. Downscaling is also necessary in weather forecast modeling, which is another area in which complex probabilistic modeling is required.

The need for scaling so that data and models are properly matched is supported by many references in different technical fields. The need to do it carefully is also critical to avoid dilution in upscaling and concentration in downscaling.

Hydrologists Blöschl and Sivapalan (1995) address scaling using a framework that distinguishes among the process scale, observation scale, and modeling scale. The observation scale is equivalent to population distribution. The model scale for PAs is much larger, requiring upscaling so that the data are properly used to represent processes that are modeled in the PA. This is, in effect, the difference between the data distribution that often represents spatial and temporal domains that are points (or very small time frames and spatial domains), and a PA model that represents very large time frames and very large spatial domains (e.g., 10,000 years, and the disposal cell). The uncertainty in the small-scaled data points is much larger than the uncertainty across much larger spatial and temporal scales.

From a statistical perspective, this is an essential consequence of the Central Limit Theorem and is like the concept of regression towards the mean. An example could include measuring the speed at which someone drives to work. Suppose the speed is recorded every minute of a 30-mile trip. Some of that time is spent at zero miles per hour (mph), such as when stopped at a stop sign or a traffic light. Some might be spent on an Interstate at 75 mph. However, the average might be 30 mph for a 30-mile trip that takes about an hour, and probably does not vary very much. The data distribution ranges from zero to 75 mph. It does not make sense to use the data distribution to represent the possible amount of time it takes to drive to work. That is, it does not ever take less than 24 minutes by traveling the whole distance at 75 mph, and it does not take forever because of being stuck at a traffic light for several minutes. That is, the work destination is achieved at some point in time. The work trip takes roughly the average of those data recorded every minute and that average does not have much uncertainty (for example, the trip takes about an hour every day). This is the impact of scaling, which is an averaging construct. Scaling needs to also be applied to data used in a PA just like it does to a model of the amount of time it takes to drive to work.

Scaling, or averaging, leads to appropriate reduction in uncertainty compared to using the data distribution. As a more relevant example, moisture content data were collected in near surface soils for a low-level radioactive waste site to support a PA in Nevada. Small samples were collected from different points in space (different locations). The measured moisture contents ranged from very low values (e.g., 3%) to large values (e.g., 30%). However, the impact of moisture content on the system performance is measured by its average, which was about 7.5%

(with a reasonable range of 7–8%). It would not make sense to model the Nevada PA with moisture content of 3% for the whole site (too dry), or of 30% (more typical of a humid site). It is the scaled distribution that is important, and that has a distribution with a range of about 7–8% given the data. The population data distribution is, typically, much broader than the scaled distribution, because scaling is a form of averaging. Another way to think about allowing use of data values in a PA instead of scaling is that it corresponds to ignoring all the other data. For example, allowing a value of 30% moisture content would mean ignoring information from all other samples that have lower values.

In this context, informing PA models with population distributions can grossly over-represent the variability of input parameters within the context of the spatial and temporal resolution of a PA model. Consequently, the development of input distributions for PA models involves scaling the available data such that larger spatial and temporal domains are characterized. Nevertheless, upscaling needs to be performed carefully to avoid risk dilution, and that care and attention has been given to the Clive DU PA.

A similar approach to scaling is used for the Tc-99 concentration data for the Clive PA. The data range from a low of about 200 pCi/g DU waste (State of Utah data) to a high of nearly 100,000 pCi/g DU waste (SRS data). Using either of these values directly in the PA would, in effect, ignore all the other data that suggest that the concentrations are somewhere between these two extremes, and would under- and over-estimate what is known about Tc-99 concentrations in DU waste. The scaled distribution has a mean of about 24,000 pCi/g of DU waste and a standard deviation of the mean (standard error of the mean) of about 11,000 pCi/g of DU waste. The relatively small reduction in variance from the data to the scaled distribution for Tc-99 reflects the differences between the three data sets available. That is, scaling is not performed without consideration of the pedigree of the underlying data. In this case, the scaled distribution is still unlikely to produce a Tc-99 concentration value of 100,000 pCi/g of DU waste; however, it could produce a value more than 50,000 pCi/g of DU waste. This is an example for which scaling is performed carefully, considering the three groups of data as separate instead of simply applying a distributional average to all the available data.

Several different approaches have been assessed to improve the representativeness of the depiction of processes with varying spatial and temporal scales in modeled systems (Arora et al. 2019; de Rooij 2011; Rödenbeck et al. 2001; Yang et al. 2017). The scaling issue can be addressed by running PA models in one of two ways: 1) by drawing random numbers from input distributions at every time step, or 2) by selecting a random realization from each input parameter distribution at the beginning of time and applying that value throughout time. These two ways of modeling are sometimes called fast and slow models in the literature on stochastic averaging, where it is understood that fast models are approximations to slow models and are formed through averaging processes (cf., Thompson et al. (2015)).

As described in the literature, including the references cited here, there are several reasons why stochastic averaging is considered necessary and appropriate, and as discussed above is consistent with hydrologic practice. Similarly, the DU PA model does not allow for approach #1 (described above) for several reasons: i. the relative computational intractability; ii. these types of models are often called "systems-level" models and are aimed at the needs of decision making under uncertainty, in which case it is uncertainty in parameters that is of importance in the context of the decision to be made; and, iii. the complications this approach causes for global (simultaneous) sensitivity analysis of a probabilistic model. Consequently, approach #2 must be used. This problem is common to all complex modeling, of which PA modeling is only one type.

With approach #2, the input distribution must reflect values that are plausible across the duration of the simulation period. Clearly, in this case, using the underlying distribution of data is inappropriate. For example, when a value representing the 99th percentile of the underlying distribution of the data is selected for use throughout the simulation period, this corresponds to a highly improbable outcome. In fact, comparing this to approach #1, where draws from input distributions are selected randomly at each time step, this corresponds to a probability of:

$$(1\text{-}0.99)^{\wedge(\text{length of simulation})}$$

If 1,000 years are simulated, this corresponds to what is effectively a zero-probability event. In fact, Microsoft Excel returns a result of zero for the function POWER(0.01,1000). Hence, when approach #2 is used, input distributions need to be scaled in such a way that there is lower variability relative to the distribution of the underlying data.

When assumptions of linearity, additivity, and stationarity are applied, then simple averaging provides an exact solution for this type of scaling. That is, characterizing the input distribution to a linear, additive, and stationary model using the mean and standard deviation of the mean (i.e., standard error) of the available data can be shown to be analytically correct. In this sense, correct implies that this approach can be shown to provide unbiased estimates for the mean and variance of the output of interest. This type of analysis helps inform the approach for scaling input distributions for parameters in PA models.

As more complex non-linear functions are considered, the results and determination of a best approach become less clear. In other words, the question becomes one of how scaling should be performed. Scaling is, in effect, weighted averaging. All weights are 1 (i.e., ordinary averaging applies) if the model is linear, additive, and stationary. It gets more complicated if they are not. PA models are not linear or additive, although they are usually treated as stationary. Scaling should then perhaps be done with something other than straight/ordinary averaging. However, there is no theoretical development yet on this. In the meantime, some type of scaling must be done.

Exploring this with both analytical and simulation approaches for non-linear functions shows that simple averaging can provide a biased estimate of the mean and variance in the output (Black et al. 2019). For example, when a quadratic function is considered, application of simple averaging results in an estimate of the mean of the process of interest that is biased by approximately 3%. Similarly, for this same case, the estimate of the variance of the process of interest is biased by approximately 2.5%. These results are consistent with the work of Vogel et al. (1991), who considered the space-time variability of soil hydraulic properties. Black et al. (2019) also explored the more general case in which the function of interest consists of the product of two independent variables. Similar results were found, indicating that using the simple averaging approach for characterizing the input distributions results in a small bias in the estimates of both the mean and the variance.

These findings provide important context regarding the use of the standard error of the mean to account for uncertainty in input parameters in the PA models. There are many complex functions and relationships embedded within PA models. Functions that are multivariate, highly non-linear, and that involve differential equations exist in PA models. Ultimately, the aggregate impact of all the functions within a PA model is the function of interest with respect to assessing the impact of different approaches to scaling.

For the GoldSim DU PA model the form of the marginal relationship between the most important/sensitive input parameters and a response of interest in a PA model lies somewhere between a linear and a quadratic (Neptune (2021c), Figures 7 and 8). That is, these types of complex models are ultimately dependent on only a few input variables for a specific endpoint. Given this, the impact of scaling with the standard error of the mean to account for uncertainty in input parameters is a slight bias in the estimation of the mean and the variance.

Ultimately, scaling of some form must be performed to avoid adversely impacting decisions, because otherwise uncertainty will almost certainly be over-estimated, perhaps severely, and PA decisions risk being made based on values from the tails of the output distributions.

There are no analytical solutions for upscaling for non-linear non-additive models. PA models tend to be highly non-linear and highly multiplicative. This issue has been recognized more generally (see references cited above as examples), and research in this area continues to be performed in various institutions around the world. However, for now there are no simple solutions. Neptune will continue to perform its own research in this area and has made breakthroughs with the use of a novel statistical approach, but this research is not complete. For the current DU PA GoldSim model, completed several years ago, the best available methods were used; not much has changed since then, especially with respect to PA in general.

As noted in NUREG/CR 6805 (Neuman et al. 2003), upscaling is necessary. Also, simple averaging tends to be a very powerful process, in which case the complexity of PA models might include trade-offs in negative and positive bias so that the center of the probabilistic output is reasonable.

Tail behavior in the output of non-linear multiplicative PA models is probably more adversely affected than the centers of the output distributions, but there are other issues in PA modeling related to lack of correlation structure that probably create more extreme tail effects. Lack of correlation structure between input variables, and lack of autocorrelation across time, almost certainly lead to more extreme tail effects than the upscaling effect of non-linear and multiplicative relationships. Consequently, it is reasonable to consider the tails, and especially the upper tails, outside the range of reasonable results. In effect, the center of the output of PA models is probably far more reliable than the tails.

A further issue that suggests that upscaling using simple averaging might often be sufficient is that global sensitivity analysis of complex models always reveals only a few input parameters that are sensitive for a given output of a PA model. Consequently, it is scaling of those few inputs that matters the most. When addressing the few input parameters that are sensitive, the lack of analytical solutions for scaling non-linear multiplicative models is not as severe as it might at first seem. Often the response variable of interest is explained in large part by a linear relationship with the most sensitive input parameters.

In summary, complex PA models that have disparate process, observation, and modeling scales require upscaling to ensure that the models properly characterize the data when forming input distributions for the model. This issue is also addressed in NUREG/CR 6805 (Neuman et al. 2003).

For complex models such as probabilistic PA models, scaling is undertaken in current best practices to rectify spatial and temporal scale differences between processes, observations, and models. The NRC has acknowledged this as the correct approach, when done carefully, in NUREG/CR 6805.

References included above have been provided in the context of the general subject of scaling and application in hydrology and climate change modeling, with acknowledgement that the same applies in weather forecast modeling. Various authors have addressed this issue in the context of hydrology modeling. Many references in scientific literature address the need for appropriate temporal and spatial scaling.

▪ ***O-10***

Snowmelt- The current version of the cover hydrology model uses the "HYDRUS snowmelt module." The efficacy of this model for predicting snow accumulation, snow melt, and infiltration has not been demonstrated for snow melt in the Clive locale. The parameters used in the model have not been presented or justified. For the DU PA v2.0, comparisons have been made to snowmelt over short windows of time and compared to the average record. However, the accepted practice is to develop a locale-specific calibration of the snowmelt function that provides predictions of snow accumulation and snowmelt consistent with observations. An example of such a comparison is provided in the figure below, which was developed for a similar assessment of an earthen cover at a different site.

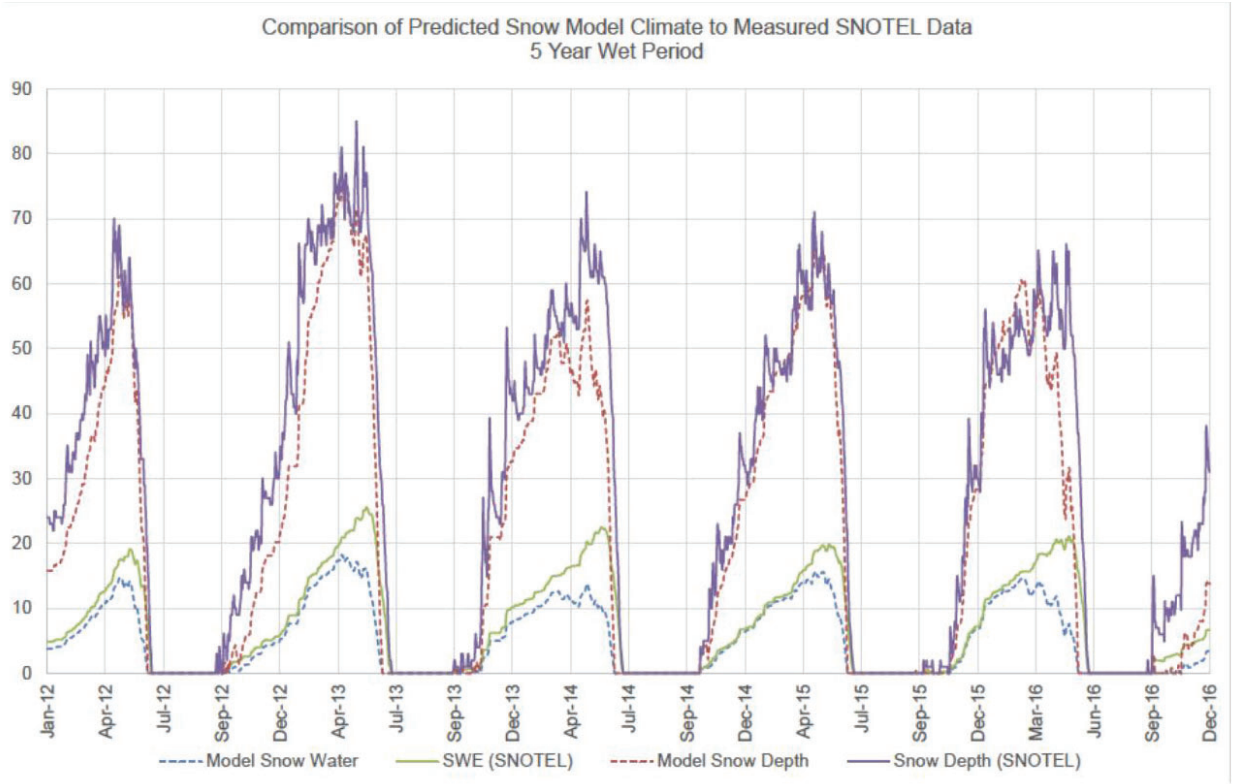

Please develop a locale-specific calibration of the snowmelt function by comparing predicted and measured snowpack over a multi-year period. Use that snowmelt algorithm in the unsaturated zone model to predict percolation from the cover.

SNOTEL data is not available for the Clive site or for a suitable analog, challenging the creation of a locale-specific calibration. Accordingly, to provide complementary lines of evidence this request is addressed in three parts: (1) a literature review; (2) an attempted site-specific validation using Cover Test Cell data; and (3) correlation of snowpack data from Dugway, UT against the snowpack predicted by applying the Dugway climate data to the HYDRUS snowmelt algorithm.

The Dugway, UT weather data does not track snow water equivalent (SWE) in the snowpack due to the site's relatively low elevation and relatively thin, non-persistent snowpack. Nonetheless, a comparable figure to that in the RFI is prepared using available data and model results.

Literature Review

A literature search was conducted to assess whether the snowmelt algorithm is consistent with current practices and has been validated for a comparable setting to Clive. The HYDRUS User Manual (Šimůnek et al. 2007) describes this algorithm as follows:

> *When heat transport is simulated simultaneously with water flow and atmospheric boundary conditions, then snow accumulation on top of the soil surface can be simulated. The code then assumes that when the air temperature is below -2 C all precipitation is in the form of snow. When the air temperature is above +2 C all precipitation is in the form of liquid, while a linear transition is used between the two limiting temperatures (-2,2). The code further assumes that when the air temperature is above zero, the existing snow layer (if it exists) melts proportionally to the air temperature.*

However, no discussion of validation of the snowmelt algorithm is provided in the HYDRUS User Manual.

The HYDRUS snowmelt infiltration routine is reported to accurately simulate snowmelt infiltration rates when compared with measured soil water content during spring thaw for the Bucegi Mountains (Dobre et al. 2017). However, this work does not include conditions representative of the Clive facility.

Similarly, Zhao et al. (2016) evaluate soil moisture and temperature simulated in HYDRUS 1D using both the snow routine and a frozen soil module against measured data for a grassland in Inner Mongolia. In this work, both the snow routine and the frozen soil module match well against measured data when the soil is not frozen, and the HYDRUS 1D frozen soil module better matches the data, particularly at an hourly level, when the soil is frozen. During times the soil is frozen, the snow routine appears to overstate soil moisture compared with the data and the frozen soil module. Summary climate data for the Inner Mongolia site is not provided, though this appears to be an arid location that could be comparable to Clive.

Cover Test Cell Model

Given indeterminate results from a literature review, the Cover Test Cell deconstruction data was looked to as a possible way to validate the HYDRUS snow routine on a site-specific basis. If HYDRUS could reasonably replicate the Cover Test Cell percolation data when the snow model was employed, the snow model would be considered sufficient for capturing the effects of snow formation and melting at the Clive, UT site.

The Cover Test Cell was constructed just south of the proposed site for the Federal Cell and was therefore exposed to all the meteorological impacts at the site, including snowfall, over the 15-year period it was monitored. The measured percolation data out of the bottom of the Cover Test Cell effectively integrated all the processes of snow accumulation and melting that would have occurred at the site during this period. Figure 1 shows the design and layering of the Cover Test Cell as it was constructed at the site.

A simplified 1D model of the Cover Test Cell is constructed in HYDRUS. The snow feature is left off in one simulation and is turned on in another. Percolation predictions from the two models are compared to actual percolation collected below the Cover Test Cell via a lysimeter tipping bucket.

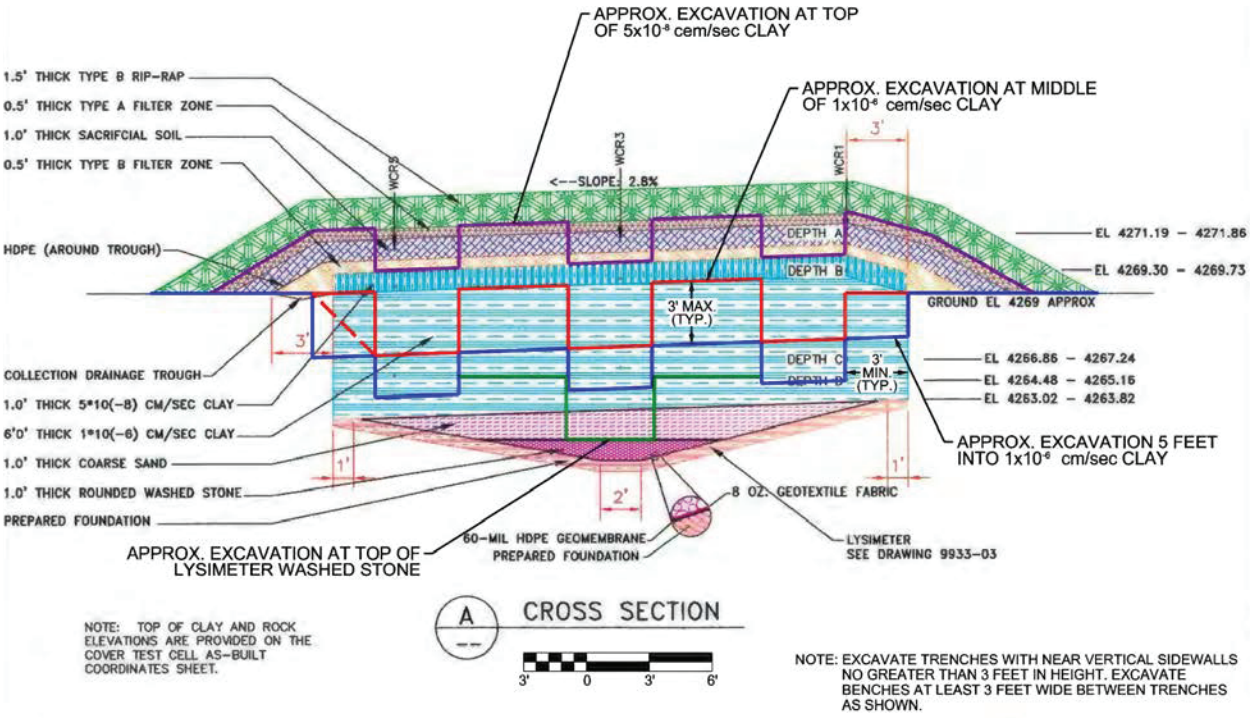

Figure 1. Cover Test Cell (reprinted from EnergySolutions (2020)).

Model Domain

A 1D column is used to model the Cover Test Cell. Seven layers are used in the 1D Test Cell model, shown in Figure 2. Because extremely coarse materials (i.e., riprap) are problematic to model when paired with an atmospheric boundary (typically requiring very small mesh refinement and/or timesteps, both of which are impractical at the scale of the 1D model and length of simulation), the material hydraulic parameters for the riprap layer are assigned the default parameters available in HYDRUS for sandy loam in the first 15.2 cm (6 in), and sand in the next 30.5 cm (12 in), as shown in Figure 2. Default parameters available in HYDRUS are based on Carsel and Parrish (1988).

With this parameterization of the riprap material, K_{sat} is high enough that no runoff occurs throughout the simulation, and therefore all precipitation is accounted for in the model domain. In addition, water content in these layers generally stays below 10%, and therefore no significant storage occurs in these layers using this parameterization.

Table 1 summarizes hydraulic properties used in the simulation. Hydraulic properties for the remaining layers are taken from Energy*Solutions* (2020). The Filter A, Sacrificial Soil, and Filter B layers each had a single sample taken and submitted for material hydraulic property testing, of which the results are shown in Table 1. For the clay layers, multiple samples are taken from the 5×10^{-8} cm/s ($n = 3$) and 1×10^{-6} cm/s ($n = 5$) layers of the Test Cell. A representative sample is selected for each layer, based on the sample's overall tendency toward the mean of each of the five parameters shown in Table 1.

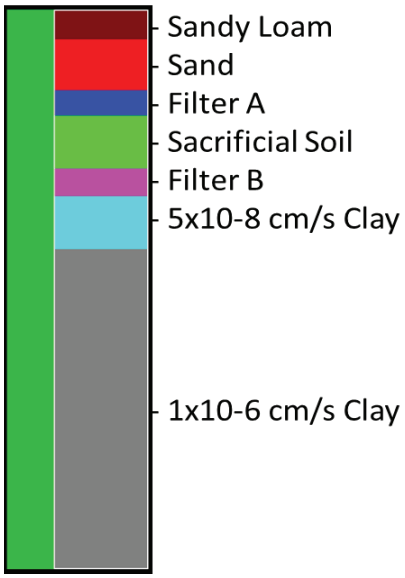

Figure 2. Layers in the 1D Test Cell model.

Table 1. Material hydraulic properties.

	Thickness cm (in)	θ_r (VWC %)	θ_s (VWC %)	α (1/cm)	n (unitless)	K_{sat} (cm/day)
Sandy Loam	15.2 (6)	0.065	0.41	0.075	1.89	106.1
Sand	30.5 (12)	0.045	0.43	0.145	2.68	712.8
Filter A	15.2 (6)	0.03	0.37	0.329592	2.79	1874880
Sacrificial Soil	30.5 (12)	0	0.3	0.0336735	1.18	24192
Filter B	15.2 (6)	0.07	0.37	0.0591837	4	907200
Upper Radon	30.5 (12)	0	0.39	0.000153061	1.39	0.00216
Lower	182.8 (72)	0	0.39	0.000132653	1.43	0.0020736

Root Water Uptake

No root water uptake is specified in the model. After passing through the "riprap" layer, water continues downward through the subsequent layers and ultimately out of the bottom of the model.

Node Resolution and Boundary Conditions

1001 nodes are used for the 320 cm (10.5 ft) 1D Test Cell model, with uniform spacing equating to approximately 3.2 mm between nodes. An atmospheric boundary condition is specified at the top node of the model and a free drainage boundary condition at the bottom node of the model.

Atmospheric Input

The same 100year repeating atmospheric record used in the DU PA v2.0 modeling is used for the 1D Test Cell model, including daily precipitation and calculations of potential evaporation. This 100-year record is repeated 10 times to run the 1D model out to 1,000 years. Over this period, the HYDRUS model obtains a quasi–steady state equilibrium, from which the percolation results are based. Two simulations are performed: one with the snow model turned off, and another with the snow model turned on.

Initial Conditions

A pressure head of -500 cm was specified for all layers as an initial condition.

Results

Percolation results are calculated as the average percolation out of the system for the last 100 years of the simulation to avoid any transient fluxes early in the simulation associated with initial conditions and are presented in Table 2. Actual percolation data from the Cover Test Cell was

collected via a tipping bucket lysimeter beneath the Cover Test Cell for a 15-year period from 2002 through 2016. Monthly total tips are shown in Figure 3, with one tip corresponding to approximately 4.74 cm^3 (0.289 in^3) of water. After dividing the measured volumes by the area of the Test Cell, an average percolation rate of 0.2 mm/yr was recorded by the lysimeter tipping bucket.

Table 2. Results of the 1D Test Cell model.

Model	Percolation (mm/yr)
With snow turned off	2.14
With snow turned on	5.32

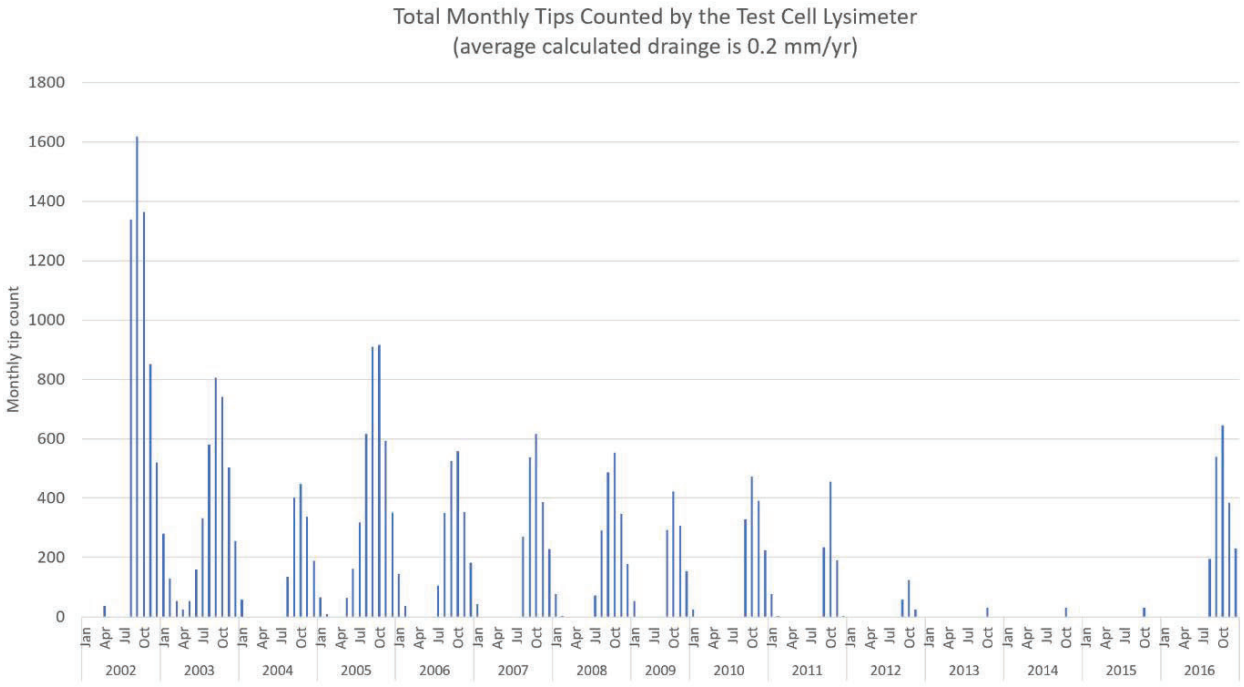

Figure 3. Monthly tip data collected from the Cover Test Cell.

Discussion

Compared with measured data, HYDRUS overpredicts percolation through the Cover Test Cell by more than an order of magnitude in both models. However, there are several additional mechanisms that occurred in the Test Cell that are not accounted for in the 1D Test Cell model. Figure 1 indicates that the 5×10^{-8} cm/s and 1×10^{-6} cm/s clays are in direct contact with adjacent subsurface native clays, and no membrane was placed at this boundary to prevent lateral flow. The Cover Test Cell deconstruction report states that it was assumed that only vertical flow of water would occur in the Test Cell. This is likely not a valid assumption, given how the Cover Test Cell was constructed.

Potential evaporation in the high desert environment at Clive exceeds annual precipitation by a large margin, leading to extremely dry conditions in the shallow soil environment. In contrast, the buried portion of the Cover Test Cell (5×10^{-8} cm/s and 1×10^{-6} cm/s clays) likely had higher water content compared to the surrounding soils because it was constructed of very coarse materials at the surface, which have little storage capacity to hold on to and return water to the atmosphere via evaporation, resulting in higher levels of percolation.

This is observed in the side slope portion of the hybrid cover model (Energy*Solutions* 2020). Placing highly conductive materials with low storage capacity at the surface allows water to quickly pass through the shallow depths and continue to deeper portions of the column where it is not subject to evaporative processes. This was likely the case with the Cover Test Cell, where increased downward flux of water through the riprap ultimately led to higher water content (and lower tension) in the 5×10^{-8} cm/s and 1×10^{-6} cm/s clays, compared to the surrounding native clays. The difference in pressure heads and water content between the clays in the Cover Test Cell and the surrounding native clays would result in a hydraulic gradient, creating lateral flow.

Simply put, one of the apparent reasons that the Cover Test Cell data did not record as much percolation per year as the 1D HYDRUS models predict is that a portion of the infiltrated water was likely leaving the system laterally and was therefore unaccounted for by the tipping bucket lysimeter.

Another reason that the percolation data from the Cover Test Cell is lower than that predicted by the 1D HYDRUS model could be the result of the establishment of vegetation and minor rooting in some of the layers of the Cover Test Cell. In the 1D HYDRUS models, no root water uptake is specified in the model. However, during deconstruction of the Cover Test Cell, a small amount of rooting was observed in the sacrificial soil layer (Energy*Solutions* 2020). Even a small number of roots in the system could lead to significant amounts of water being captured and returned to the atmosphere via transpiration. Benson (2021) has shown the effectiveness of even minor amounts of rooting on the performance of covers constructed with riprap at the surface.

Lastly, Figure 1 shows a "collection drainage trough" on the left side of the diagram. The aim of this trough was to capture any excess water that did not travel downward into the 5×10^{-8} cm/s clay (the Cover Test Cell diagram indicates a 2.8% slope, and therefore some lateral flow at this boundary was expected). The data collected from this trough, however, was deemed to be of poor quality and to not be reliable, and therefore could not be used in a mass balance calculation. Despite the actual data not being useful in a quantitative sense, there was reasonable assurance that this trough did collect some amount of water over the 15-year period of monitoring. It is likely that a portion of the water infiltrating through the Test Cell left the system through the collection drainage trough and was therefore unaccounted for by the lysimeter tipping bucket data.

Accordingly, the Cover Test Cell system is poorly suited for modeling with a simple 1D column, and attempting to address the snowmelt question via this pathway is inconclusive.

Comparison with Regional Snowpack Data

An analysis is presented here that evaluates how well the HYDRUS snowmelt sub-model predicts snowmelt compared with observed historical data.

Snow Accumulation and Snowmelt

The following is a brief overview of how the HYDRUS snowmelt algorithm operates. HYDRUS calculates snowmelt proportional to the air temperature using a snowmelt constant (M), which is the amount of snow (given in length units, such as cm of water) that will melt during one day for each °C. The HYDRUS model also employs a sublimation constant (S) that accounts for vaporization that is mediated by potential evaporation.

HYDRUS uses the following equation for calculation of the snow layer at time t:

$$h_t = h_{t-1} + \Delta h_t - (S)(E_t) - (M)(T_t)$$

Where:

h_t	is snow water equivalent (SWE) height of the snow layer at time t (cm)
h_{t-1}	is SWE height of the snow layer at time $t-1$ (cm)
Δh_t	is change in SWE height of the snow layer at time t due to precipitation (cm)
S	is sublimation constant
E_t	is potential evaporation at time t (cm)
M	is melting constant (cm/°C)
T_t	is average daily temperature above 0˚C; set to zero if the daily temp is < 0°C

The change in snow layer, Δh_t, is determined by the daily temperature and precipitation. If the temperature is below -2°C, all of the precipitation is assumed to have fallen as snow and adds to the snow layer. If the temperature is between -2°C and 2°C, the precipitation is assumed to have fallen as a mix of rain and snow, and Δh_t is reduced in a linear fashion. As noted above, the last term is set to zero if the daily average temperature is less than zero, as no melting is assumed to occur. Converting the SWE snow layer to actual snow depth requires an assumption of snow density; the HYDRUS manual recommends a ratio of 10:1 (i.e., 1 cm of SWE is equal to 10 cm of snow).

Daily potential evaporation (PE) is calculated with values for extraterrestrial radiation and daily maximum, minimum, and mean temperatures using the Hargreaves method (see Neptune (2021b) for details). HYDRUS default values of 0.43 for M and 0.2 for S are used in the calculation. This algorithm is applied to local climate data to evaluate the efficacy of this snowmelt algorithm that is used in HYDRUS. Daily temperature, snowfall, and snow layer data are obtained for the nearby site of Dugway, UT (site id 422257) using the SC ACIS Tool (http://scacis.rcc-acis.org/). Since HYDRUS calculates snow water equivalent, the snow layer is calculated with the rules outlined in the HYDRUS manual, which uses the ratio of 1 cm snow water to 10 cm of snow.

Snow layers are calculated for the entire Dugway record (09/21/1950 – 07/08/2013) using the HYDRUS algorithm and are then compared to the corresponding observed snow layer. Average daily calculated snow layers are plotted along with average daily observed snow layers across the entire year (Figure 4). The HYDRUS algorithm performed well, with calculated snow layers tracking along the observed values. HYDRUS does appear to overestimate compared with observed snow layers in January and to underestimate in February. These values balance out when averaged from December through February, with the calculated snow layer (0.98 cm) only slightly exceeding the observed snow layer (0.94 cm).

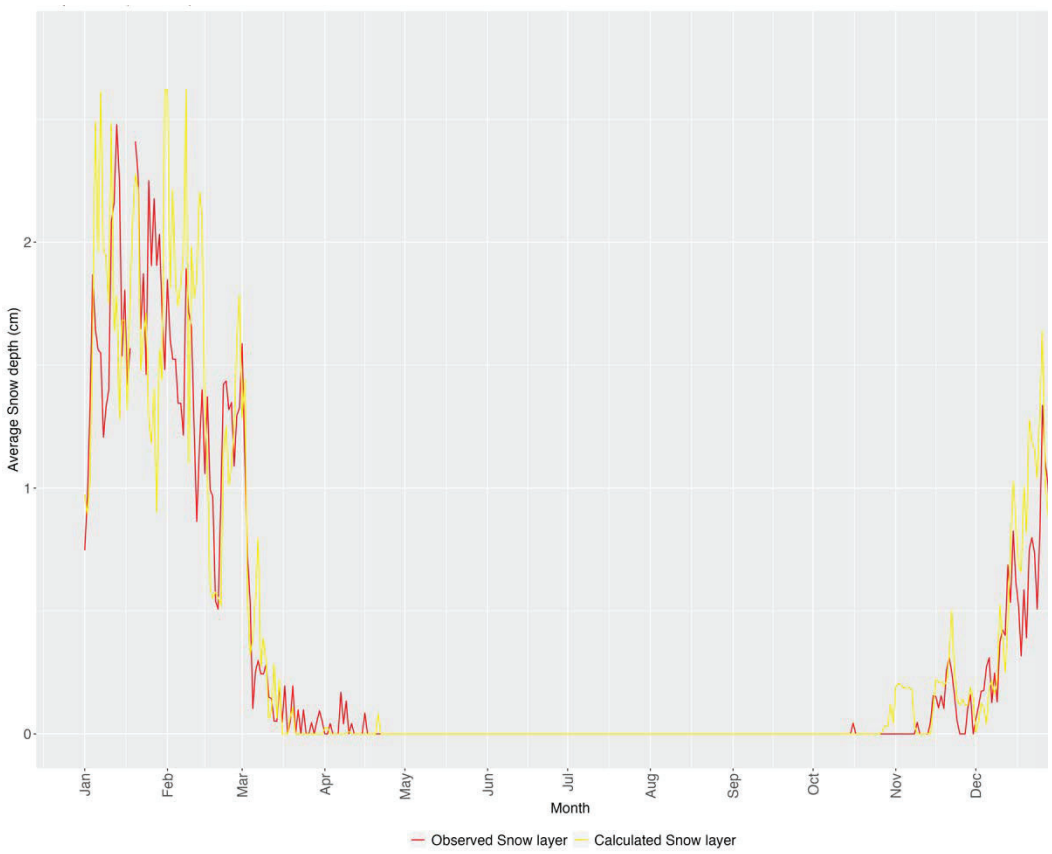

Figure 4. Average daily calculated and observed snow layers at Dugway, UT.

For a closer look, snow layers are calculated for a 5-year wet period (January 1, 1962 – December 31, 1966) in the Dugway record using the HYDRUS algorithm and are then compared to the corresponding observed snow layer. Daily calculated snow layers are plotted along with daily observed snow layers across the 5-year period (Figure 5). Additionally, calculated SWE is plotted, although there is no direct data to use as observed SWE values for comparison. The closest Snotel location is the Mining Fork Station (ID:631) at an elevation of 8,295 ft. Dugway is at 4,200 ft so Mining Fork does not provide relevant data. There are no Snotel sites located in areas that have as little annual snowfall as Dugway. Though the HYDRUS algorithm contains instances of both overestimating and underestimating during this 5-year wet period, the spikes in snow depth are often at the same time as the spikes in the observed snow depth. The Dugway dataset is missing observations for approximately 20% of the data needed for snow layer calculations. Measurements of the observed snow layer were only recorded to the nearest inch. This limits the observed snow layer measurement to be recorded in increments of 2.54 cm. Additionally, Dugway receives a nontrivial amount of snowfall in February, when average daily temperatures move above 2°C (Figure 6). Under these conditions HYDRUS does not predict snowfall. Discrepancies may also occur from differences between air and ground temperature, where warmer ground temperatures should lead to more snowmelt and less snow accumulation.

Colder ground temperatures might limit snowmelt when air temperatures begin to increase. HYDRUS does not include ground temperatures in its snow layer calculation. Seasonal lag in ground temperatures theoretically would lead HYDRUS to overestimate snow accumulation in the early part of the winter and to underestimate snow accumulation in late winter/early spring, which is consistent with the pattern seen in Figure 6.

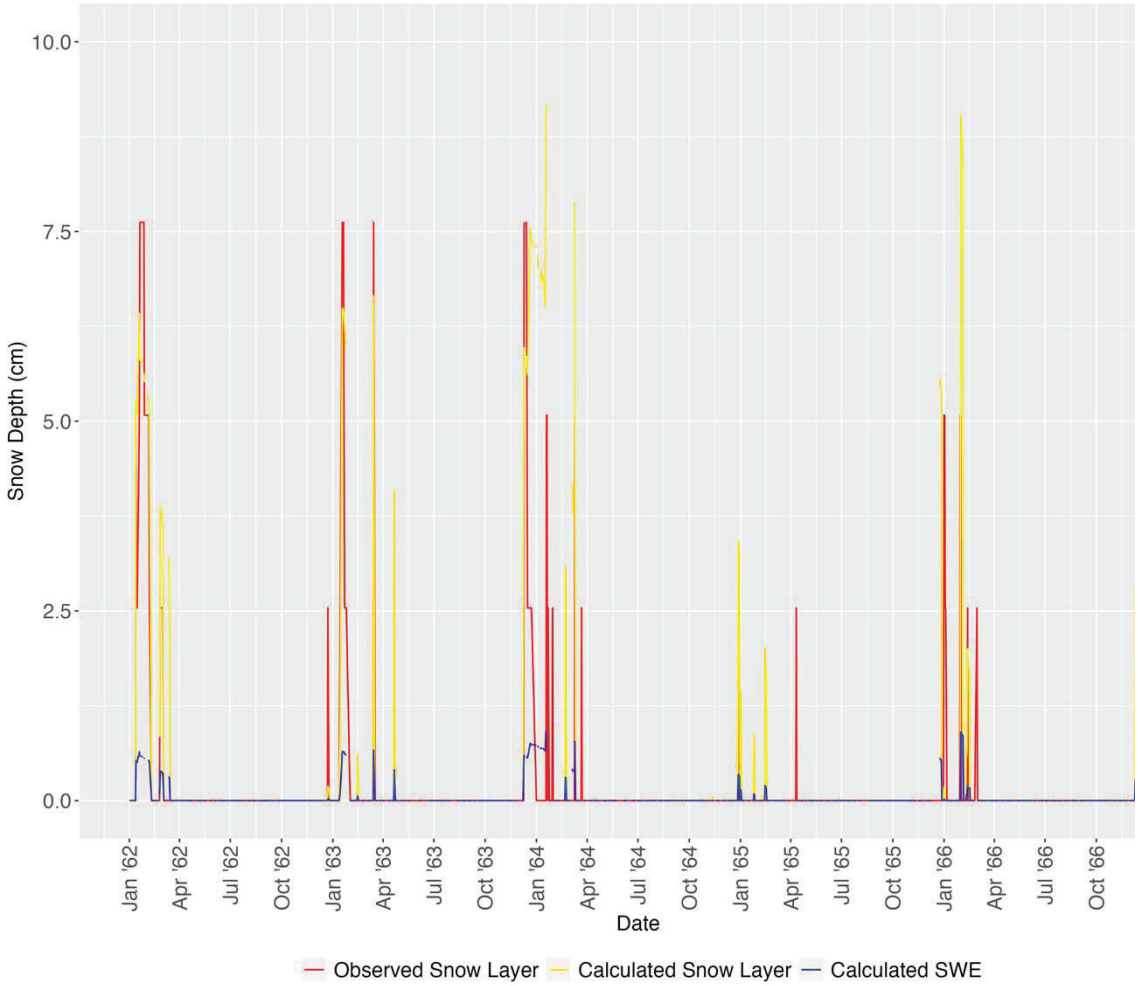

Figure 5. Daily calculated and observed snow layers and calculated SWE at Dugway, UT, January 1962 – December 1966.

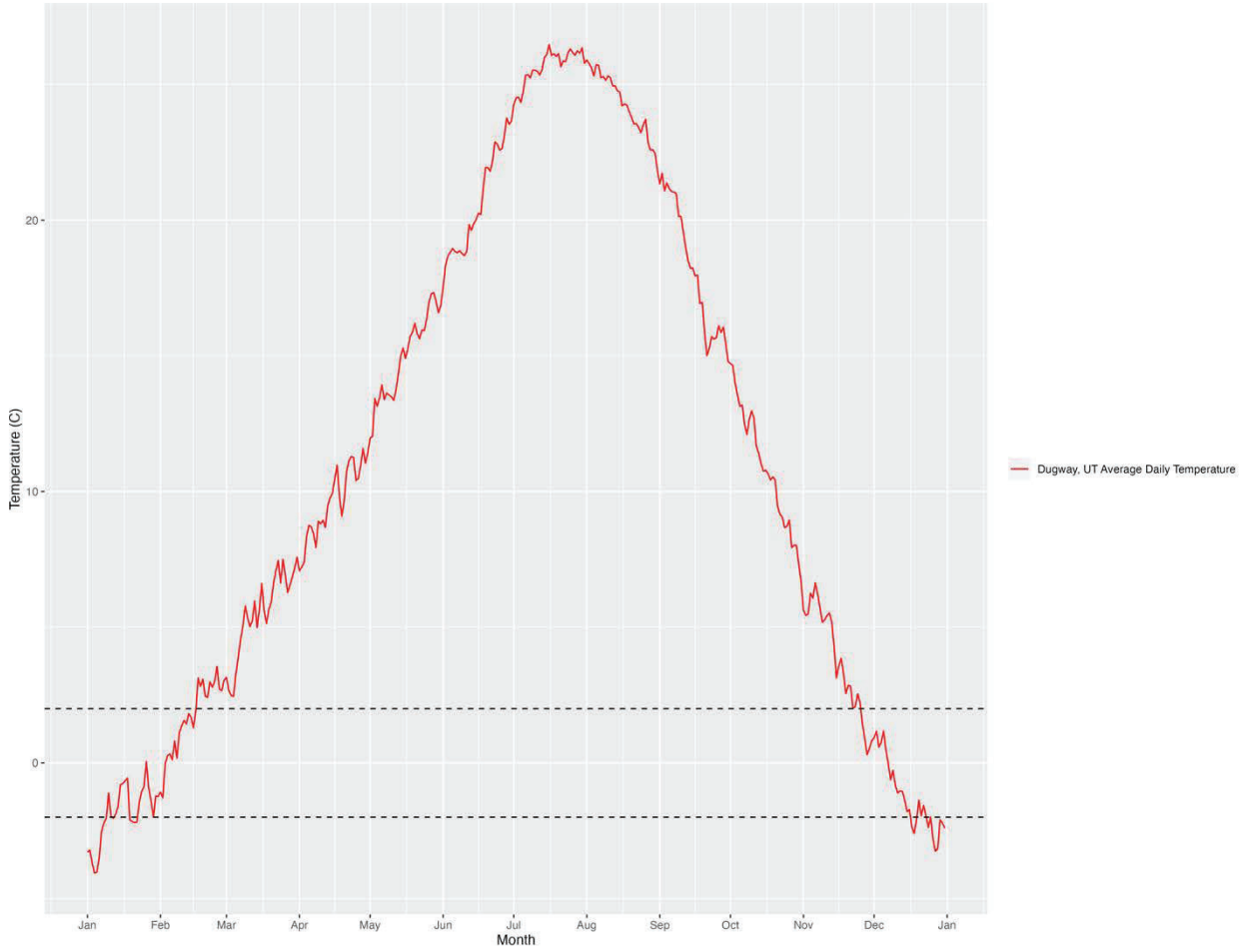

Figure 6. Daily Mean Temperature at Dugway, UT averaged across the period of record. Horizontal lines represent -2°C and +2°C

Summary

A quantitative validation of the snowmelt algorithm in HYDRUS is demonstrated by comparing HYDRUS-based snow accumulation estimates and observed snow accumulation data from Dugway. The analysis of a 5-year wet period for the Dugway site focuses attention on a critical time period for the validation of the snowmelt model in HYDRUS. In general, the snow accumulation, and corresponding snowmelt, calculated by HYDRUS tracks the observed snow accumulation from Dugway quite well. The fit of the model provides support for the assertion that locale-specific calibration would provide a negligible increase in the ability of the HYDRUS snowmelt algorithm to estimate snow depth and snowmelt dynamics. Despite small discrepancies, the average calculated snow accumulation matches the average observed snow accumulation. These analyses demonstrate the efficacy and sufficiency of the snowmelt algorithm utilized by HYDRUS. Collectively, these analyses help demonstrate that the HYDRUS snowmelt sub-model

properly predicts snow accumulation and snowmelt, and hence infiltration, measured soil-water content, and soil-water storage at various depths.

▪ ***O-11***

Flow Mechanisms and Model Validation- The HYDRUS model used for the evaluation of final cover over the Federal Cell considers only hydraulically driven flow. However, thermally driven flows often are predominant relative to hydraulically driven flows in semi-arid and arid regions like Clive, Utah, particularly for depths greater than 0.3 m (Scanlon 1994; Scanlon and Milly 1994). For example, at the White Mesa site in Blanding, Utah, thermally driven mechanisms have been found to be the predominant mechanism responsible for percolation, yielding percolation rates on the order of 0.6 to 0.8 mm/yr. Evaluate the significance of thermally driven flows in the final cover over the Federal Cell, and compare the magnitude of thermally driven flows to the hydraulically driven flows predicted with the HYDRUS model.

> ▪ ***Scanlon, B., 1994, Water and Heat Fluxes in Desert Soils, 1. Field Studies: Water Resources Research, 30(3), pp 709-719***
> ▪ ***Scanlon, B. and Milly, P., 1994, Water and Heat Fluxes in Desert Soils, 2. Numerical Simulations: Water Resources Research, 30(3), pp 721-733.***

The directive refers only to thermally driven flows. However, the cited references only consider thermal gradients with respect to the flow of water vapor. Scanlon and Milly (1994) note in their explanation of the governing flow equation that:

> D_{Ta} is the transport coefficient for adsorbed liquid flow due to thermal gradients, which is ignored in this study because we believe it is negligible in comparison with D_{Tv} [thermal vapor diffusivity]. (Scanlon and Milly 1994)

Thus, the directive appears to be requesting an evaluation of multiphase water flow subjected to both hydraulic and thermal gradients. While the question states definitively that thermally driven flows are shown to be dominant in the cited studies, the studies themselves are more cautious in their conclusions. Scanlon and Milly (1994) describe a modeling effort using field data documented in Scanlon (1994). The model showed a downward thermal vapor flux during the one-year simulation period that resulted in increased water storage at depth. The study acknowledged several limitations and noted that this modeling result was not confirmed with field data:

> There are insufficient data available to determine whether the net downward thermal vapor flux was balanced by storage change or liquid flux in the field. (Scanlon and Milly 1994)

The study also acknowledges significant uncertainties with respect to the unsaturated hydraulic conductivity functions which might have restricted countervailing upward liquid flow, concluding:

> This annual cumulative downward water flux indicates that the model is not in equilibrium with its atmospheric forcing. This could indicate true disequilibrium in the field, or it may be attributable to inaccuracies in hydraulic conductivities, which may underestimate upward liquid fluxes. (Scanlon and Milly 1994)

A more recent modeling study of vadose zone flow in several semi-arid and arid sites in response to long-term climatic forcing (Scanlon et al. 2003) showed that predicted thermal vapor fluxes were often upward. The figure below (Figure 7), reproduced from Scanlon et al. (2003), shows the breakdown of liquid and vapor fluxes for the four modeled sites. None of the sites showed long-term downward thermal vapor fluxes (denoted V_T in the figures).

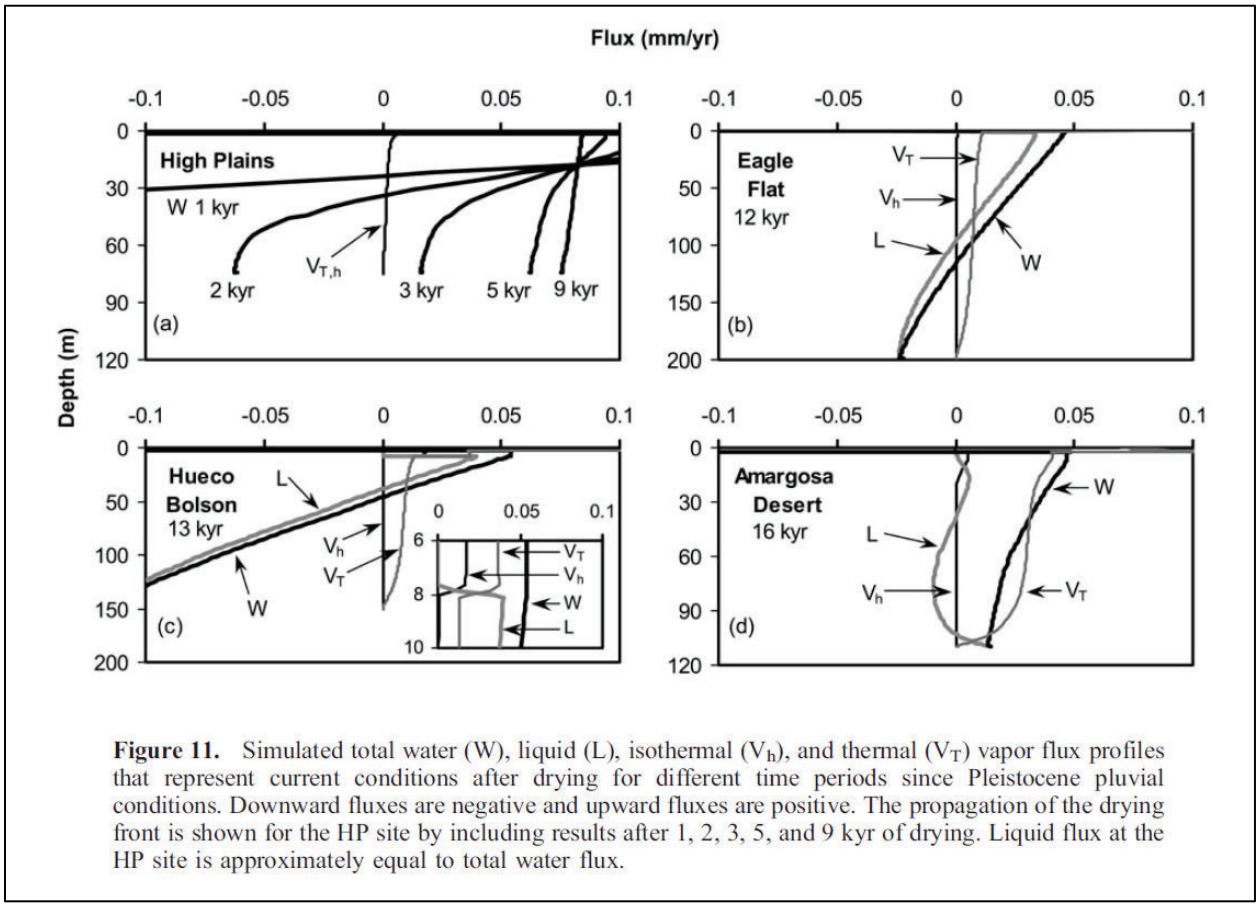

Figure 11. Simulated total water (W), liquid (L), isothermal (V_h), and thermal (V_T) vapor flux profiles that represent current conditions after drying for different time periods since Pleistocene pluvial conditions. Downward fluxes are negative and upward fluxes are positive. The propagation of the drying front is shown for the HP site by including results after 1, 2, 3, 5, and 9 kyr of drying. Liquid flux at the HP site is approximately equal to total water flux.

Figure 7. Magnitude of liquid and vapor fluxes from Scanlon et al. (2003), Figure 11.

A set of simulations was performed to estimate the influence of vapor fluxes (both isothermal and thermally driven) in the ET cover. These simulations used the built-in functionality of HYDRUS 1D, which is the same code used by Scanlon et al. (2003) and uses analogous governing equations to those documented in Scanlon and Milly (1994). See Scanlon et al. (2003) and Šimůnek et al. (2005) for a detailed discussion of the governing equations, including the dependence of the vapor diffusion coefficient with temperature.

The model setup was identical to the DU PA v2.0 model (discretization, material assignments, atmospheric forcings, etc.). Thermal properties were assigned using the built-in properties selector in HYDRUS. The frost protection layer was assigned the "Sand" properties, while the remaining layers were assigned thermal properties for "Clay." A zero-gradient temperature boundary condition was selected for the bottom of the model. The resulting temperature fluctuations in the soil column mimic those observed in the Cover Test Cell, though the cover systems are not identical and the atmospheric forcings in the model were from the synthetic 1000-year meteorological record described in the DU PA Model v2.0. Temperature response to the atmospheric forcing was most pronounced near the surface and was muted and delayed in the lower layers. Note also that location TH-1 in the Cover Test Cell was located 4.5' below the surface, at the base of the layer of $5x10^{-8}$ cm/sec (upper) radon barrier clay. The upper radon barrier clay in the Federal Cell is at the same depth below the surface. Figure 8 and Figure 9 show data from the Cover Test Cell deconstruction report (Energy*Solutions* 2017) and the thermal modeling results (Simulation 1002), respectively.

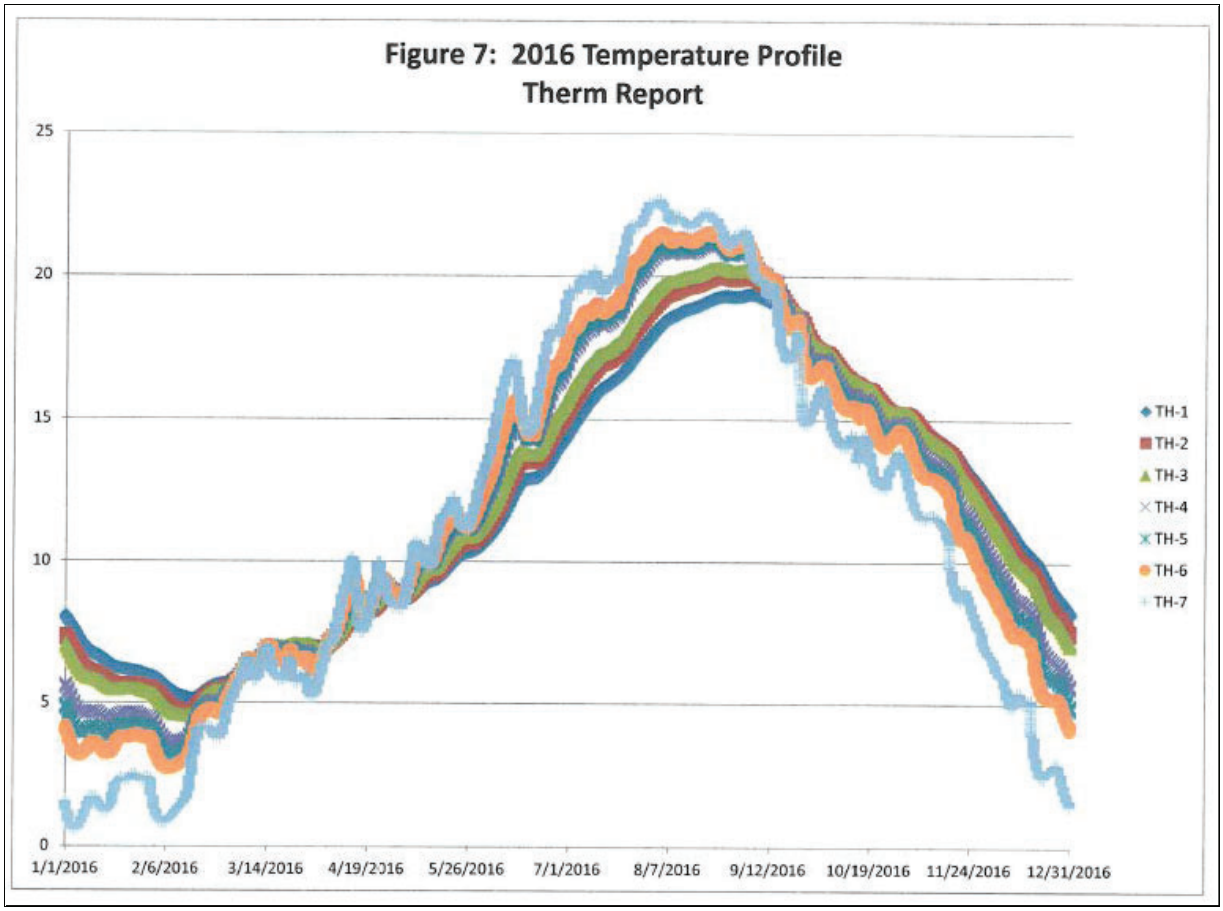

Figure 8. Temperature data at various depths in the Clive Cover Test Cell from EnergySolutions, 2017 Figure 7.

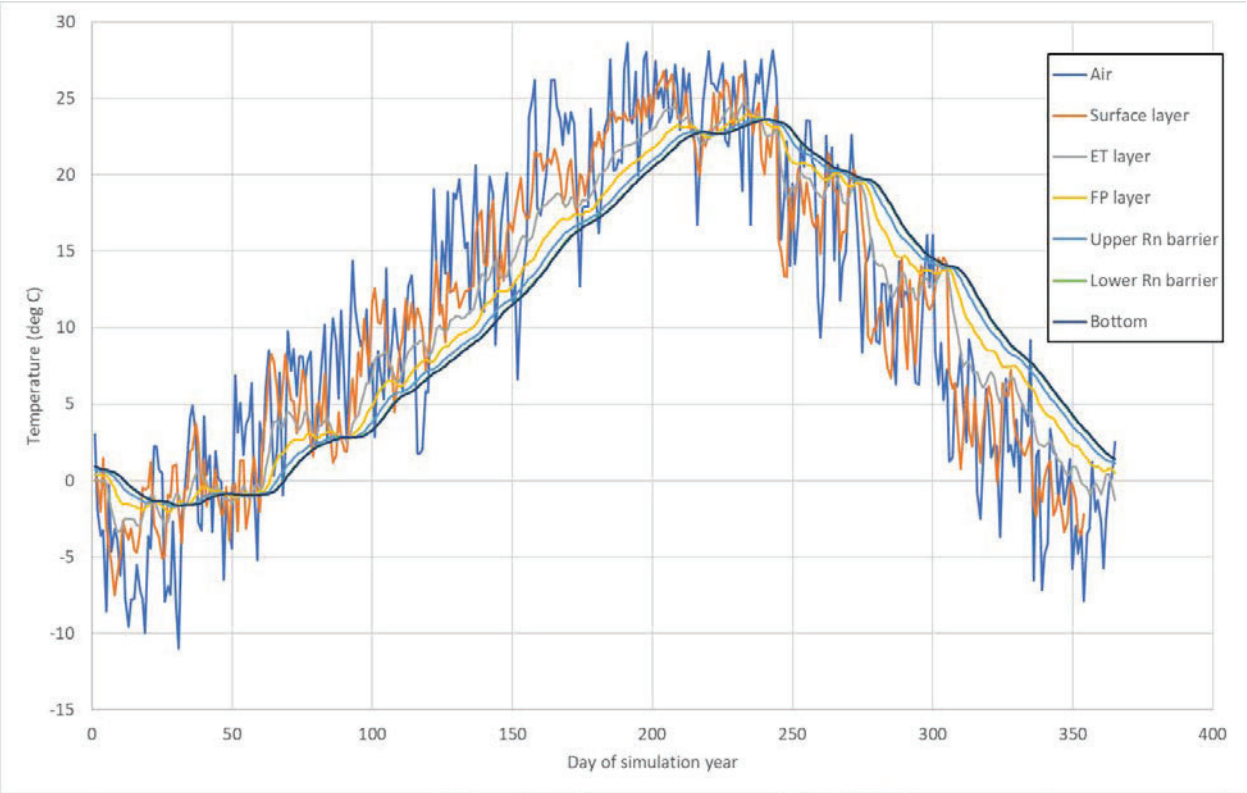

Figure 9. Simulated temperature data at various depths in Simulation 1002 (vapor flow and temperature flow simulated).

Simulations were run for 100,000 days (~274 years), which includes a significant storm cycle just before day 80,000. Figure 10 shows the cumulative fluxes at the bottom of the domain. Four parameter sets were run in the model v2.0 setup (denoted "base" in the legend) and a separate run using vapor flow and heat transport (denoted "Vapor+Thermal" in the legend). Results show that adding vapor and heat transport processes to the model resulted in reduced cumulative drainage in two of the four parameter sets (1002 and 0005), while two showed increased cumulative drainage (0551 and 0353).

To understand the relative magnitudes of liquid flux, thermally driven vapor flux, and isothermal vapor flux, four flux profiles are presented in Figure 11 for two times in simulations 0005 and 0353. These times correspond to before and after the notable increase in cumulative drainage evident in the previous figure at around 80,000 days. The left panel of each figure shows all three fluxes; in all cases, the liquid fluxes are much higher than the vapor fluxes. The right panels exclude the liquid flux to highlight the vapor flux profiles. Thermal vapor fluxes are generally

much larger than isothermal vapor fluxes at these times. Vapor fluxes of both types reduced markedly at the interface with the radon barrier at a depth of around 107 cm, where the air-filled pore space is lower due to the persistently higher water content.

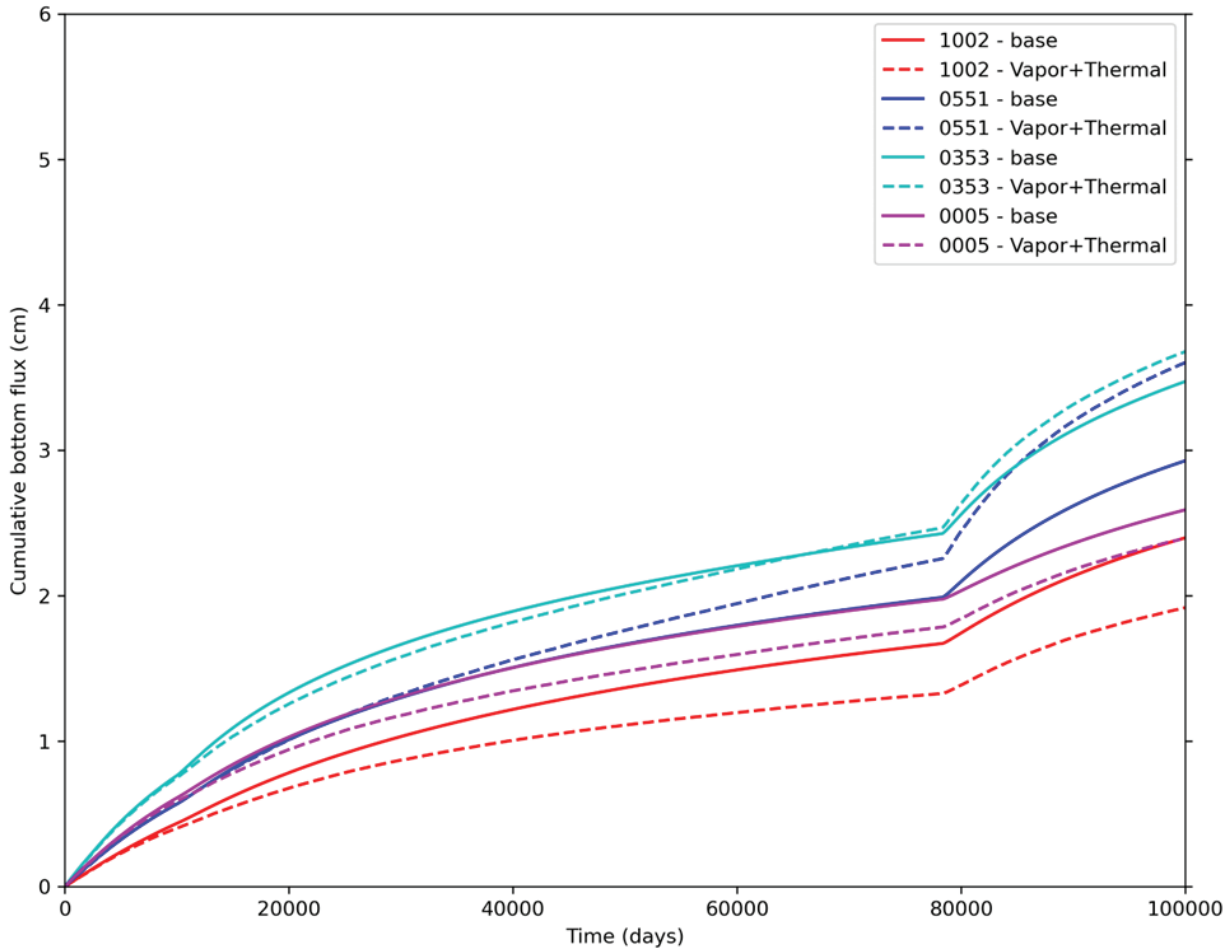

Figure 10. Cumulative fluxes at the bottom of the HYDRUS 1D profile for four simulations from the DU PA v2.0, with temperature and vapor flow enabled.

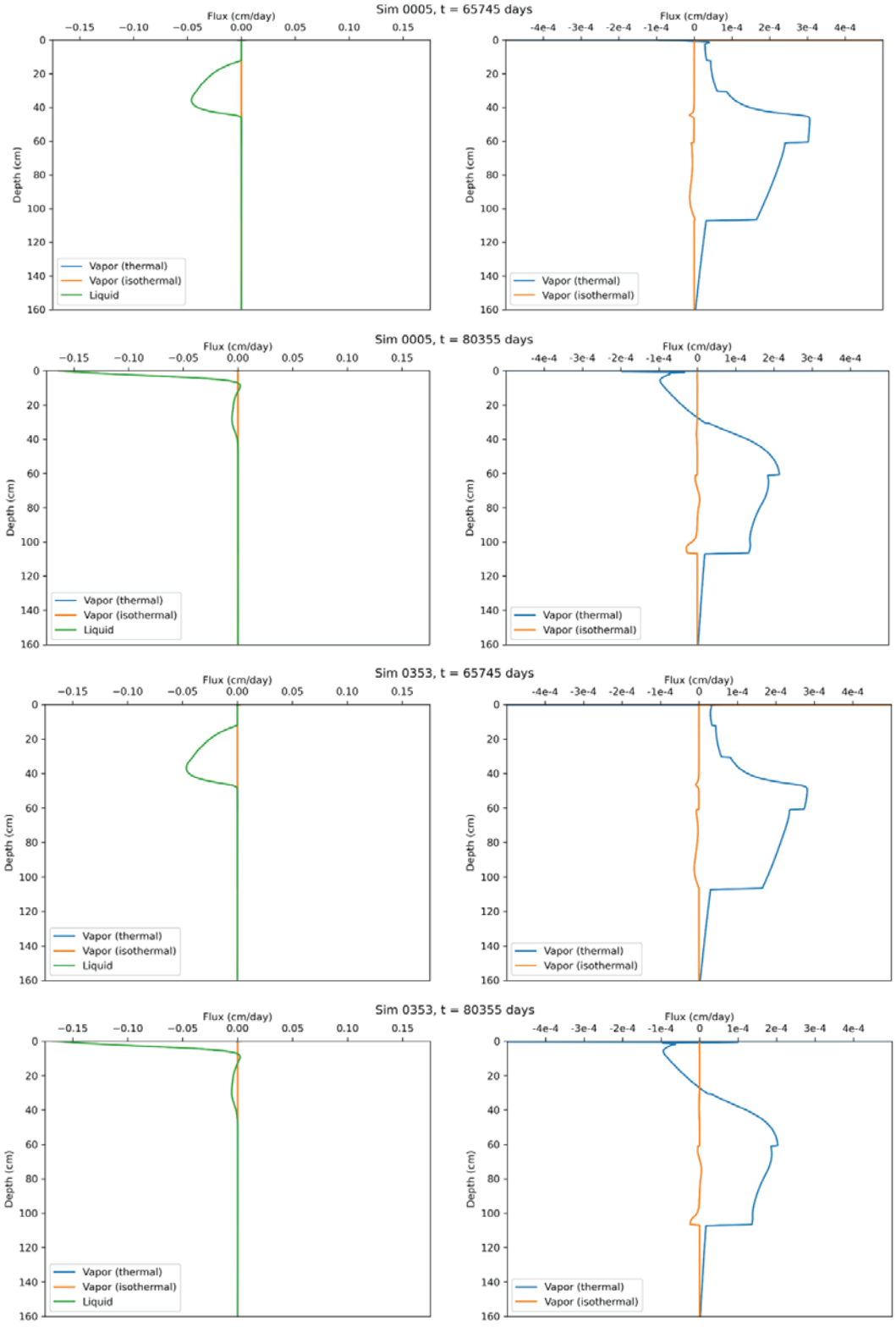

Figure 11. Fluxes for two simulations, before and after a large drainage event.

These simulations suggest that vapor movement due to thermal gradients can impact percolation through the cover system. However, the impacts to net flow through the cover were not consistent for the simulations. Where cumulative flow through the cover increased, the magnitude was not significant enough to impact the general conclusions of the DU PA v2.0 Model.

▪ ***O-12***
Hydraulic Properties Measurement and Reporting- The unsaturated zone analysis relies heavily on the hydraulic properties cited in Bingham (1991) for water retention and hydraulic conductivity. These engineering properties are used extensively in the unsaturated zone analysis, but only scant documentation has been provided regarding how these properties were measured and whether the measurement techniques used in the late 1980s or very early 1990s provided engineering properties consistent with the current standard of care for engineering design. Provide the report issued by the Colorado State University Porous Media Laboratory that is cited in the report by Bingham Environmental (1991), including documentation on the procedures that were followed by the laboratory. Describe how the methods that were used by the Colorado State University Porous Media Laboratory are consistent with accepted industry standards for measuring the unsaturated hydraulic properties of earthen materials for use in engineering design, such as ASTM D6836 (Standard Test Methods for Determination of the Soil Water Characteristic Curve for Desorption Using Hanging Column, Pressure Extractor, Chilled Mirror Hygrometer, or Centrifuge1) and ASTM D7664 (Standard Test Methods for Measurement of Hydraulic Conductivity of Unsaturated Soils). Describe the representativeness of these properties to field conditions associated with the Federal Cell, including scaling phenomena.

> ▪ ***Bingham Environmental, 1991, Hydrogeologic Report, Envirocare Waste Disposal Facility South Clive, Utah: Prepared for Envirocare of Utah, Salt Lake City, UT, October 9, 1991.***

The unsaturated zone analysis initially consisted of several HYDRUS model runs that were largely reliant on Bingham Environmental (1991) in terms of material properties. For DU PA v2.0 and beyond, Neptune has developed methods to complete 1,000 HYDRUS model runs using input distributions for important material properties. Accordingly, the current analysis incorporates multiple lines of evidence and testing to inform hydraulic properties and is not strictly reliant on Bingham Environmental (1991). For example, much useful data has been generated with the Cover Test Cell deconstruction project completed in 2019 (Energy*Solutions* 2020). However, the Cover Test Cell was constructed to an earlier version of the rock armor cover design used at the Clive facility; therefore, only data for the radon barrier clays is comparable between the Cover Test Cell and the evapotranspiration (ET) cover proposed in the DU PA. Considering that similar

material properties were used for the surface/evaporative zone and radon barrier layers in the DU PA, some comparison can be made with these layers as well.

NUREG/CR-7028 (Benson et al. 2011) provides recommendations in its Section 10.2 regarding engineering properties for fine-textured earthen storage and barrier layers that can be used in performance assessments in lieu of site-specific data. These recommendations are based on covers studied 5 to 10 years after initial construction. The Cover Test Cell was deconstructed, and its material properties tested 18 years after it was placed into service (for a roughly comparable, if longer, period of system stabilization and naturalization to that evaluated in NUREG/CR-7028).

Table 3 summarizes engineering properties across the HYDRUS modeling performed in DU PA v2.0 (Neptune (2021b), Table 10), the Cover Test Cell, and NUREG/CR-7028. Average values are calculated in any cases where a range of values are provided in the source documentation and are discussed in more detail below.

Specifically, in the HYDRUS modeling supporting the DU PA, the parameters of K_{sat}, α, and n were varied for the surface layers, all parameters were varied for the frost protection layer, and K_{sat} was varied for the upper and lower radon barrier layers. Any other parameters were deterministic (Neptune 2021b).

For the Cover Test Cell, all radon barrier values represent the average of three (for the upper radon barrier) to five (for the lower radon barrier) data points, as reported in the Energy*Solutions* (2020) appendix "Wisconsin Geotechnical Laboratory, Hydraulic Properties of Soils from a Final Cover Test Section in Clive, Utah, Geotechnical Laboratory Report No. 20-17, 2020; Table 1." The Cover Test Cell also returned data for that cover design's riprap, filter zone, and sacrificial soil layers; however, the material properties for these layers do not match the ET cover design so these data are not included in Table 3.

Values for NUREG/CR-7028 reflect the average of the recommended range in Section 10.2, or the recommended initial condition for PA modeling. NUREG/CR-7028 recommended values are applied to both the surface/evaporation zone and radon barrier layers. NUREG/CR-7028 does not suggest values to use for a layer such as the frost protection layer, which provides a capillary break within the cover system.

Table 3. Engineering properties of cover layers for DU PA v2.0, the Cover Test Cell, and NUREG/CR-7028.

		Design Basis		
Layer	**Input Parameter**	**ET Cover DU PA v2.0**	**Cover Test Cell**	**NUREG/CR-7028**
Surface	θ_r (unitless)	0.111	*n*/a	0[3]
	θ_s (unitless)	0.4089	*n*/a	0.4
	α (1/cm)	Variable	*n*/a	0.0204
	n (unitless)	Variable	*n*/a	1.3
	K_{sat} (cm/day)	Variable	*n*/a	22
Evaporative Zone	θ_r (unitless)	0.111	*n*/a	0
	θ_s (unitless)	0.481	*n*/a	0.4
	α (1/cm)	Variable	*n*/a	0.0204
	n (unitless)	Variable	*n*/a	1.3
	K_{sat} (cm/day)	Variable	*n*/a	22
Frost Protection	θ_r (unitless)	Variable	*n*/a	*n*/a
	θ_s (unitless)	Variable	*n*/a	*n*/a
	α (1/cm)	Variable	*n*/a	*n*/a
	n (unitless)	Variable	*n*/a	*n*/a
	K_{sat} (cm/day)	Variable	*n*/a	*n*/a
Upper Radon Barrier	θ_r (unitless)	0.1	0	0
	θ_s (unitless)	0.432	0.38	0.4
	α (1/cm)	0.003	0.0002	0.0204
	n (unitless)	1.172	1.39	1.3
	K_{sat} (cm/day)	Variable	5.16E-03	22
Lower Radon Barrier	θ_r (unitless)	0.1	0	0
	θ_s (unitless)	0.432	0.38	0.4
	α (1/cm)	0.003	0.0002	0.0204
	n (unitless)	1.172	1.4	1.3
	K_{sat} (cm/day)	Variable	1.13E-02	22

[3] Inferred from Table 6.3 of NUREG/CR-7028 for all clay layers, though not explicitly discussed in Section 10.2 therein.

Several observations can be made from Table 3. All comparisons are limited to the surface/evaporative zone and radon barrier layers since there are not comparable data in the Test Cell or NUREG/CR-7028 for the frost protection layer.

In DU PA v2.0, the value for θ_r is higher than that reported for the Cover Test Cell and inferred from NUREG/CR-7028. Benson et al. (2011) commonly report a value of zero for θ_r for all soil types. Benson's laboratory also evaluated the soil properties from the Test Cell, and therefore θ_r is reported to be zero for these soils as well. However, other well-used and well-known soils databases (e.g., Rosetta, Carsel and Parrish (1988)) do not report zero values of θ_r The effect of using a zero value for θ_r is to increase the storage capacity of the soil. In addition, a zero value of θ_r will also affect the water content at which percolation occurs.

Values for θ_s and n are comparable across these approaches/data sets, while the value for α used in DU PA v2.0 is comparable to that in NUREG/CR-7028 for the surface/evaporative zone layers. For the radon barrier layers, the value for α used in DU PA v2.0 is bracketed by those demonstrated by site-specific Cover Test Cell data and those recommended by NUREG/CR-7028, with the Cover Test Cell data being roughly an order of magnitude lower than modeled, and NUREG/CR-7028 roughly an order of magnitude higher than modeled. Therefore, the α used in DU PA v2.0 is nicely bounded by site-specific data and the "generic" value of α informed by multiple datasets in NUREG/CR-7028.

Finally, values for K_{sat} vary widely between those reported by site-specific Cover Test Cell data and those used in DU PA v2.0 and recommended by NUREG/CR-7028. The latter two values are roughly comparable, while the site-specific data is three to four orders of magnitude lower. The site-specific K_{sat} is very low because of construction specifications and demonstrates little change from the as-built condition over the Cover Test Cell's 18-year service life.

▪ ***O-13***

Hydraulic Properties Parameterization- The unsaturated zone analysis relies heavily on hydraulic property functions that apparently were parameterized, in part, using water retention and hydraulic conductivity data reported in Bingham Environmental (1991). Documentation on how these parameters were determined has not been provided and in some cases the parameters that have been employed are inconsistent with the current standard of care in engineering practice for hydrologic design. For example, the residual water content, representing the lowest water content that can be realized, is assigned values commensurate with a water saturation on the order of 30%. Similarly, the pore interaction term is assigned a single value of 0.5 based on information nearly five decades old (i.e., Mualem 1976), whereas more recent information suggests that the pore interaction term should be assigned different values depending on soil texture (Schapp and Leij 2000, Benson and Bareither 2012).

- ***Bingham Environmental, 1991, Hydrogeologic Report, Envirocare Waste Disposal Facility South Clive, Utah: Prepared for Envirocare of Utah, Salt Lake City, UT, October 9, 1991.***
- ***Benson, C. and Bareither, C., 2012, Designing Water Balance Covers for Sustainable Waste Containment: Transitioning State-of-the-Art to State-of-the-Practice: in K. Rollins and D. Zekkos, eds, State of the Art and Practice in Geotechnical Engineering, Keynote Lectures from GeoCongress 2012, GSP No. 226, ASCE, Reston VA, 1-32.***
- ***Mualem, Y., 1976, A new model predicting the hydraulic conductivity of unsaturated porous media. Water Resources Research, 12, pp 513–522.***
- ***Schaap, M., and Leij, F., 2000, Improved Prediction of Unsaturated Hydraulic Conductivity with the Mualem-Van Genuchten Model: Soil Science Society of America Journal, 64(3), pp 843-851.***

This item raises concerns relating to data derived from Bingham Environmental (1991). The unsaturated zone analysis initially consisted of several HYDRUS model runs that were largely reliant on Bingham Environmental (1991) in terms of material properties. For DU PA v2.0 and beyond, Neptune has developed methods to complete 1000 HYDRUS model runs using input distributions for important material properties. Accordingly, the current analysis incorporates multiple lines of evidence and testing to inform hydraulic properties and is not strictly reliant on Bingham Environmental (1991). For example, much useful data has been generated with the Cover Test Cell deconstruction project completed in 2019 (Energy*Solutions* 2020). However, the Cover Test Cell was constructed to an earlier version of the rock armor cover design used at the Clive facility; therefore, only data for the radon barrier clays is comparable between the Cover Test Cell and the evapotranspiration (ET) cover proposed in the DU PA. Considering that similar material properties were used for the surface/evaporative zone and radon barrier layers in the DU PA, some comparison can be made with these layers as well.

NUREG/CR-7028 (Benson et al. 2011) provides recommendations in its Section 10.2 regarding engineering properties for fine-textured earthen storage and barrier layers that can be used in performance assessments in lieu of site-specific data. These recommendations are based on covers studied 5 to 10 years after initial construction. The Cover Test Cell was deconstructed, and its material properties tested 18 years after it was placed into service (for a roughly comparable, if longer, period of system stabilization and naturalization to that evaluated in NUREG/CR-7028).

Table 3 summarizes engineering properties across the HYDRUS modeling performed in DU PA v2.0 (Neptune (2021b), Table 10), the Cover Test Cell, and NUREG/CR-7028. Average values are calculated in any cases where a range of values are provided in the source documentation and are discussed in more detail below.

Specifically, in the HYDRUS modeling supporting the DU PA, the parameters of K_{sat}, α, and n were varied for the surface layers, all parameters were varied for the frost protection layer, and K_{sat} was varied for the upper and lower radon barrier layers. Any other parameters were deterministic (Neptune 2021b).

For the Cover Test Cell, all radon barrier values represent the average of three (for the upper radon barrier) to five (for the lower radon barrier) data points, as reported in the Energy*Solutions* (2020) appendix "Wisconsin Geotechnical Laboratory, Hydraulic Properties of Soils from a Final Cover Test Section in Clive, Utah, Geotechnical Laboratory Report No. 20-17, 2020; Table 1." The Cover Test Cell also returned data for that cover design's riprap, filter zone, and sacrificial soil layers; however, the material properties for these layers do not match the ET cover design so these data are not included in Table 3.

Values for NUREG/CR-7028 reflect the average of the recommended range in Section 10.2, or the recommended initial condition for PA modeling. NUREG/CR-7028 recommended values are applied to both the surface/evaporation zone and radon barrier layers. NUREG/CR-7028 does not suggest values to use for a layer such as the frost protection layer, which provides a capillary break within the cover system.

Several observations can be made from Table 3. All comparisons are limited to the surface/evaporative zone and radon barrier layers since there are not comparable data in the Test Cell or NUREG/CR-7028 for the frost protection layer.

In DU PA v2.0, the value for θ_r is higher than that reported for the Cover Test Cell and inferred from NUREG/CR-7028. Benson et al. (2011) commonly report a value of zero for θ_r for all soil types. Benson's laboratory also evaluated the soil properties from the Test Cell, and therefore θ_r is reported to be zero for these soils as well. However, other well-used and well-known soils databases (e.g., Rosetta, Carsel and Parrish (1988)) do not report zero values of θ_r. The effect of using a zero value for θ_r is to increase the storage capacity of the soil. In addition, a zero value of θ_r will also affect the water content at which percolation occurs.

Values for θ_s and n are comparable across these approaches/data sets, while the value for α used in DU PA v2.0 is comparable to that in NUREG/CR-7028 for the surface/evaporative zone layers. For the radon barrier layers, the value for α used in DU PA v2.0 is bracketed by those demonstrated by site-specific Cover Test Cell data and those recommended by NUREG/CR-7028, with the Cover Test Cell data being roughly an order of magnitude lower than modeled, and NUREG/CR-7028 roughly an order of magnitude higher than modeled. Therefore, the α used in DU PA v2.0 is nicely bounded by site-specific data and the "generic" value of α informed by multiple datasets in NUREG/CR-7028.

Finally, values for K_{sat} vary widely between those reported by site-specific Cover Test Cell data and those used in DU PA v2.0 and recommended by NUREG/CR-7028. The latter two values are roughly comparable, while the site-specific data is three to four orders of magnitude lower. The site-specific K_{sat} is very low because of construction specifications and demonstrates little change from the as-built condition over the Cover Test Cell's 18-year service life.

▪ **O-14**

Hydraulic Properties of Frost Protection Layer- The unsaturated zone analysis of the final cover relies heavily on the capillary break assumed to form between the evaporative zone layer and the frost protection layer. No information is provided to indicate how the hydraulic properties of this layer were determined, and whether they are consistent with the materials available for construction. Provide documentation on how the hydraulic properties of the frost protection layer, which also serves as a capillary barrier, were measured, how variability in the hydraulic properties of the frost protection material was characterized, and how the hydraulic property functions were parameterized.

The request in O-14 is addressed in two parts: (1) properties of the Frost Protection Layer (FPL); and (2) long-term durability of the FPL as a distinct layer over the compliance period of the Federal Cell.

FPL Properties

Material hydraulic parameters for the cover layers, including the FPL, used in DU PA v2.0 are summarized in Table 3. Greater detail is provided in section 12.5.2 of Neptune (2021a), which summarizes the process used to generate distributions around possible material properties for the FPL. Analysis of the source material for the FPL indicated that about 75% of the fines content was sand (Energy*Solutions* 2021a), while the percent silt and percent clay of the remaining 25% were not measured. These properties were varied over 1000 simulations in HYDRUS in order to model a variety of possible conditions.

There are two purposes of the FPL. One is to protect layers below the FPL from freeze/thaw cycles and wetting/drying cycles, and to inhibit plant, animal, or human intrusion (Neptune 2021b). The second purpose is to create a strong capillary barrier that will deter downward infiltration from the surface and evaporative layer into the FPL. Smesrud and Selker (2001) and many other studies have shown that a cover design with a fine-grained layer over a coarse-grained layer provides a strong capillary barrier to restrict the flow of water.

The FPL consists of particles ranging in size from 16 inches to clay size particles. In the HYDRUS model used with the DU PA v1.4 GoldSim model, the FPL was modeled as a sandy loam because a sandy loam represents a coarse-grained material with some silt and clay (Neptune

2021b). Hydraulic properties of sandy loam for the FPL were selected using the HYDRUS hydraulic properties pull-down menu, which use properties from the Carsel and Parrish (1988) database of hydraulic parameters.

In order to evaluate the efficacy of the FPL in the DU PA modeling, a what-if scenario HYDRUS model was built using all properties from the Clive DU PA HYDRUS model, but with the cover layering, cover thickness, and cover hydraulic properties taken from the tailings cover design for the White Mesa Mill Site near Blanding Utah (MWH Americas 2007).

The cover design from MWH Americas (2007) was selected because the two sites (Clive and White Mesa) are similar in climate and setting, but the White Mesa design does not have a strong capillary barrier (with a fine layer over a coarse layer). Average annual precipitation at Blanding and Clive is approximately 13.3 and 8.3 inches per year, respectively; the Blanding site has about 60% more precipitation than the Clive site.

MWH Americas (2007) report an average flux rate through the cover system of 1E-4 cm/day (0.4 mm/yr). When the White Mesa cover layering, cover thickness, and cover hydraulic properties are used with all other components of the Clive DU PA HYDRUS model, the percolation out of the bottom of the cover is 1.2 mm/yr, which is two orders of magnitude higher than the average annual percolation for the 50 DU PA v.1.4 HYDRUS simulations (0.02 mm/yr). It is notable that, even with less precipitation at the Clive site, percolation was higher at the Clive site with White Mesa layering than that reported for the White Mesa study (0.4 m/yr).

The results of this what-if scenario model exercise demonstrate the effectiveness of the FPL in the Clive DU PA cover design.

Long-Term Durability of the Frost Protection Layer

Part 2 is addressed by considering the following question: Assuming distinct layers are present at the time of construction, is it reasonable to expect that those layers will persist over geologic time?

In short, given the environmental and geological conditions at the Clive site, it is likely the FPL will persist. Note also that the bank run material to be used for the FPL is mined from a gravel pit located at an outcrop a few miles north of the site. These materials have persisted as a distinct deposit since the beginning of the current interglacial climate cycle some 11.6 thousand years ago (Neptune 2021d).

An assessment of the stability of distinct layers in the cover at the Clive site begins with a review of a similar evaluation of an analog at the Hanford site. The Hanford and Clive sites share important similarities that are relevant to the potential for soil layers to mix, hence making Hanford a reasonable analog for the Clive site. At Hanford, Bjornstad and Teel (1993) found that natural processes (deflation, compaction, illuviation, cryoturbation, bioturbation) did not pose a

significant threat over the next 1000 years to the stability of engineered barriers. Their assertion regarding the lack of threat to the stability of the layers within an engineered barrier was based on: 1) the arid to semi-arid desert environment, and 2) the location of the site within a basin where significant eolian deposition of fine-grained silt occurs. These are the critical features that Clive and Hanford have in common with respect to the stability of geologic layers.

Both Clive and Hanford are situated in arid to semi-arid desert environments. The arid climates correspond to low primary productivity, relatively sparse insect and mammal activity and, hence, minimal bioturbation. SWCA (2011) observed limited density of diversity of vegetation with average plant species cover consisting of: 14.3% black greasewood, 5.9% Sandberg bluegrass, 3% cover each of shadscale saltbrush and gray molly. Importantly, observed ground cover was dominated by 79.2% biological soil crust, which provides an effective stabilization for the soil surface. These studies also found that root densities were largely concentrated near the surface of the soil, with few large, woody roots encountered in deeper soils. Rooting depths were shallow, with the maximum rooting depth of dominant woody plant species ranging from 16 to 28 inches. Consequently, plants have negligible impacts on soil turnover.

The density and diversity of burrowing animals including ants and mammals are also limited by the environmental conditions at the Clive site. SWCA found a low density of ant and mammal burrows with an average of 24 ant mounds per hectare (9.7 per acre), with anthills covering 4.6% of the ground surface in field study sites (SWCA 2012). Most of the below ground ant nest volume is within 24 inches (60 cm) of the soil surface due to the presence of compacted clay and caliche layers. Ant nest volume and corridor densities generally decrease with depth with most of the activity occurring in the upper layers.

Within the survey, four categories of mammal burrows were identified: ground squirrels, kangaroo rats, mice/rats/voles, and one badger. Kangaroo rats and the mice/rats/voles represent most identified burrows, with only two burrows associated with ground squirrels and one badger burrow identified. For the PA model, maximum burrow depth was set at 200 cm based on best professional judgment (Neptune 2021c). This depth is consistent with that used at Nevada National Security Site (NNSS) by Neptune (2005), and represents the likely average vertical extent of multiple badger excavations (Kennedy et al. 1985). Mammal burrows on average are much shallower and, at the Hanford Site, small mammals generally do not burrow below 10 inches (25 cm) depth (Bjornstad and Teel 1993). Although badgers are capable of burrowing to depths over 2 m, it is thought that most “badger burrows” are enlargements of small mammal burrows that were further excavated in pursuit of prey (Bylo et al. 2014). Collectively, the results of these site-specific plant and animal surveys provide strong evidence that Clive, like Hanford, has little exposure to meaningful mixing of soil layers from either plant or animal activity.

Both Clive and Hanford are in arid to semi-arid desert environments that reside in basins with significant eolian deposition of fine-grained silt. Neptune evaluated the nature, thickness, and thickness variations of eolian sediments at the upper part of the sedimentary section in nine excavated sections at the Clive site on December 15 to December 17, 2014 (Neptune 2015).

The degree of soil development in the eolian silt is gradational through the deposits indicating soil formation contemporaneous with eolian deposition. The primary mode of eolian deposition at the Clive site is deposition of fine-grained silt from suspension fallout during episodic windstorms (Neptune 2015). Well-developed soil horizons are not superimposed on the upper part of the eolian section. This conceptual model is supported by an analysis of a near continuous record of eolian deposition and a lack of soil formation preserved at the Clive site since the regression of Lake Bonneville below the Clive elevation (approximately 13,500 years before present (B.P.)). (See Figure 12, taken from Neptune (2015)). Ultimately, aeolian deposition acts fast enough that true soil horizons cannot form.

In summary, survey data from the site suggest that there are no plant or animal mechanisms to disturb surface soil layers. This is consistent with analysis conducted for similar purposes at the analog Hanford site. An additional similarity with the analog Hanford site is the significant aeolian deposition that prevents formation of soil layers. Together, these two factors strongly preclude the existence of any plausible mechanism that would significantly mix the layers of a cover. This conceptual model is supported by the work shown from analyses performed on the site (Figure 12). Ultimately, given the environmental and geological conditions at the Clive site, it is considered likely that the FPL will persist.

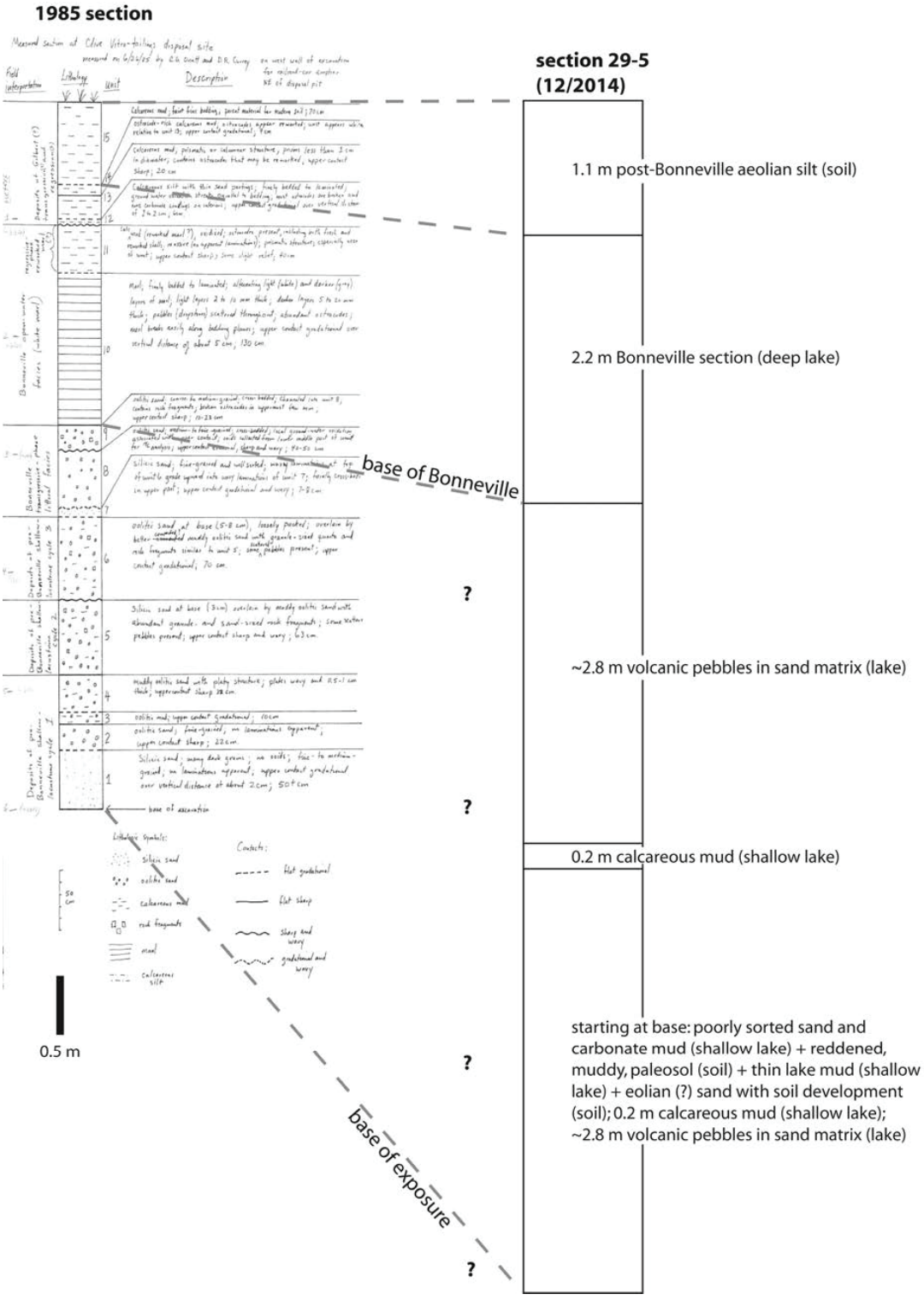

Figure 12. Reproduced from A.1 Clive Pit Wall Interpretation (C. G. Oviatt, unpublished data) and stratigraphic comparison with quarry wall studies from Neptune (2021d).

▪ ***O-15***

Soil Cover Fraction- The earthen cover for the Federal Cell relies on evapotranspiration (ET) to remove water that infiltrates and is stored within the cover profile. The dynamics and timing of infiltration, water re-distribution, and ET influence deep penetration of water and percolation from the base of the cover. Appendix O indicates that a unique soil cover fraction (SCF) was assigned to partition evapotranspiration (ET) into evapotranspiration (E) and transpiration (T) for each of the 1000 realizations. Describe how the SCF was varied temporally during the growing season and over longer periods of time in response to variations in meteorological conditions. If the SCF was time invariant, provide justification for using a single SCF to describe the time varying process and describe how this affects predictions of percolation and water content within the cover profile. Additionally, provide documentation that the SCF methodology is applicable and has been validated for partitioning ET in vegetative communities in arid regions. This information will provide the information needed to evaluate assumptions made when formulating and parameterizing the model, and the impact of the assumptions on the predictions.

A constant vegetative soil cover fraction (SCF) value is applied in the unsaturated zone modeling used for the Clive DU PA. HYDRUS 2D/3D is used to model unsaturated flow through the Federal Cell cover as a response to environmental forcings (precipitation, ET, radiation, etc.) at the land surface. An SCF value is used by HYDRUS to assign a fraction of the total prescribed potential evapotranspiration (PET) to be available for two separate mechanisms that return water to the atmosphere in the model: evaporation potential (Ep), which reflects the potential for evaporation to occur at the soil surface, and transpiration potential (Tp), which represents the fraction available for plants to transpire. While the modeled PET varies temporally, following a roughly annual sinusoidal curve reflecting changes in seasonal insolation, the value for SCF is held constant throughout each simulation. To incorporate the uncertainty of the SCF parameter on overall cover performance, SCF values are randomly drawn from a distribution of probable values for 1000 unique HYDRUS simulations, based on site-specific vegetation cover studies. Simulations are run for 2000 years, and the results from the last 1000 model years are used to determine average drainage out of the bottom of the cover.

In semi-arid ecosystems, vegetative growth is typically limited by the availability of moisture. In semi-arid climates, soil moisture pulses in winter last much longer than in summer, due to reduced PET (Schwinning and Sala 2004). However, the length of winter at Clive is limited, with the majority of the year having greater daily PET compared to precipitation (Neptune 2021b). Significant pulses of moisture into the soil from precipitation are typically lacking during the warmer months and die-back occurs for plants that are not drought tolerant. Here the magnitude of potential seasonal variability in SCF at Clive is examined to assess whether it is sufficiently captured in the existing distribution of SCF values used in the HYDRUS simulations.

Annual average precipitation at Clive ranges from 10–25 cm, with most precipitation occurring in late winter and early spring (SWCA 2012). Therefore, there is typically a single season of vegetative growth in the spring when moisture is available, and PET is moderate. Into the summer and through the fall, precipitation is sparse, and die-back of non-drought tolerant species occurs, while native perennials can persist through these dry periods due to their deep rooting. Field studies of sites analogous to the Clive site reflect vegetation communities characteristic of Greasewood Flat and Mixed Salt Desert Scrub. The sites were found to be dominated by sparsely distributed halophytic shrubs, with very limited distribution of grasses or forbs (SWCA 2012), except where recently disturbed. The design of the vegetated cover for the Federal Cell is such that the vegetation community on the cover should reflect the surrounding ecosystem.

For semi-arid ecosystems dominated by xeric perennial species, observed seasonal changes are often small in comparison to landscapes dominated by annual species. Remote sensing was used to quantify temporal changes in vegetation cover in an analogous arid environment of the Negev Desert of Israel (Schmidt and Karnieli 2000). The study found that the fraction of vegetation cover from perennial species was largely invariant through time, and that overall seasonal differences in vegetation cover could be attributed primarily to the growth of annual species. Looking at the Great Basin, U.S., Bradley and Mustard (2005) compared the inter-annual variability in a landscape dominated by cheatgrass (an annual species) to that found in landscapes composed of native perennial shrubs and bunch grass. The study found that native perennial shrubland ecosystems in the Great Basin were more adapted to variable amounts of rainfall, due to greater rooting depths. Normalized Difference Vegetation Index (NDVI) was used to estimate total vegetation cover through time, and seasonal fluctuations were approximately four times greater in cheatgrass areas compared to those observed in native shrub landscapes.

A study of the semi-arid Owens Valley, California (Elmore et al. 2003) found that the percent live cover of xeric vegetation annually changed less than +/-5%, acknowledging that this was not much greater than the error of measurement (3.8%), despite observed changes in precipitation of up to 20 cm between years. In contrast, percent live cover in areas dominated by exotic annuals changed +/- 20% with a similar variability in precipitation. Camacho-De Coca et al. (2004) estimated the total variability in SCF (across all vegetation types) in many semi-arid landscapes in Portugal and France, and reported that, for sparse shrub dominated landscapes, the fraction of vegetated cover (FVC, equivalent to SCF) changed only by 10% between dry and wet seasons.

Since the vegetation community on the Federal Cell is expected to be dominated by perennial shrubs, with limited annual grasses and forbs, the seasonal variability in total vegetated soil cover fraction is expected to be low, on the order of around 5–10% according to the studies cited above from analogous sites. The large fraction of xeric perennial species expected at the site indicates that the SCF should remain relatively constant throughout the year, and that a constant value is likely suitable in a probabilistic modeling context. While a constant value is used throughout each individual simulation, the full distribution of probable values is explored through 1000 unique simulations.

The objectives of the 2012 field studies (SWCA 2012) were to select sites such that all potential vegetation types within the target elevation range were captured, but to also include variations in aspect and slope. The variability in site characteristics resulted in a wide range of total percent cover of vegetation across the eight plots. Estimates of total canopy cover across the sites ranged from 5.8–39.5%. Additionally, the 2012 field studies were carried out in late June, which can be assumed to be well after the winter pulse of moisture. The timing of the surveys is such that they should not have been substantially biased by ephemeral early season growth of annuals. The estimates of SCF from the field studies therefore represent the portion of the vegetation cover expected to be present at the site during the majority of the year. As such, perennial species (saltbush, bluegrass, seablite, and greasewood) accounted for about 85% of the cover measured at the field study plots (SWCA 2012).

Given the small temporal variability expected in perennial vegetation at the Clive site and the large range of SCF values incorporated in distribution for SCF, the distribution spans a much larger range of SCF values (random values selected for the 1000 HYDRUS runs ranged from 0.05 to 0.28) compared to any seasonal temporal variability that might be expected at the site. SCF is estimated to change up to approximately +/-10% throughout the year, with higher fractions occurring in the spring when moisture is available, and less occurring during summer through late fall when moisture is scarce. Therefore, any uncertainty in potential seasonal variability of SCF within a single simulation is accounted for in the wide range of SCF values explored across the 1000 HYDRUS simulations. This wide range of values used in the probabilistic runs of HYDRUS provides a better account and reflection of uncertainty in SCF at the site than any seasonal variability that may occur.

▪ ***O-16***

Water Balance Graphs and Water Content Records- The reliability of predictions from a variably saturated flow model used to predict the hydrology of an earthen cover depends on whether the model accurately captures soil water dynamics and redistribution within the cover in response to a broad range of hydrological conditions. Provide water balance graphs, corresponding to ten 3-year periods during the 1000-yr simulation that correspond to ten different hydrologic conditions over 3-year periods that (i) are much wetter than normal, (ii) are much drier than normal, (iii) contain one or more extreme events with high liquid precipitation, (iv) contain one or more extreme events with high frozen precipitation, and (v) are representative of typical conditions. These graphs will be used to evaluate the reliability of the predictions. A water balance graph is a line graph showing cumulative water balance quantities (precipitation, runoff, lateral flow, evapotranspiration, and percolation) along with soil water storage as a function of time. An example of such a water balance graph from Benson (2017) is provided below. In these graphs, include two different lines for soil water storage: soil water storage in the materials above the radon barrier and soil water storage in the radon barrier. Provide a water content graph to complement each water balance graph that is a line graph showing the water content at mid-depth in each layer as a function of time.

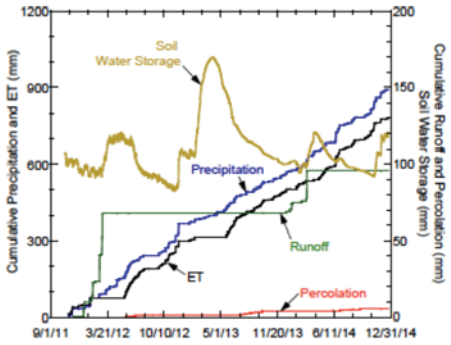

▪ Benson, C., 2017, Using Principles of Unsaturated Soil Behavior to Design Water Balance Covers for Waste Containment: Case Study: in Hoyos, J. McCartney, S. Houston, and W. Likos, eds, *Proc. PanAm Unsaturated Soils 2017, Plenary Papers, GSP No. 300*, L.., ASCE, Reston VA, pp 306-324.

Water balance graphs along with corresponding water content graphs are provided in Attachment 1, which is included at the end of this RFI O-16 response. In additional to all requested information, the water balance graphs include the simulated snow layer depth to aid in interpretation, especially for the periods of high snow accumulation. Similarly, the water content graphs include the daily percolation at the bottom of the cover system.

The graphs are provided for the five conditions requested during one realization of the HYDRUS 1-D model. Two periods were selected for each condition, making a total of ten water periods. The methodology for choosing the periods for each condition is provided below.

i) Wet periods were identified by examining the 3-year rolling average of water storage in the column as a function of time. Periods of high-water storage were selected. (Wet Period 1 and Wet Period 2 in Attachment 1.)
ii) Dry 3-year periods were identified in the same manner as wet periods. Times corresponding to low 3-year rolling average of total water storage were chosen. (Dry Period 1 and Dry Period 2 in Attachment 1.)
iii) High rain periods were selected such that one period includes the highest single day of precipitation (High Rain Period 1 in Attachment 1), and the other period includes successive high precipitation events, including the highest average precipitation over a 30-day period (High Rain Period 2 in Attachment 1).
iv) High snow periods were selected by examining the meteorological input record to find periods of significant snow accumulation. Both periods selected include multiple snow events with snow accumulations more than 5 cm snow-water equivalent. (High Snow Period 1 and High Snow Period 2 in Attachment 1.)
v) Periods of typical moisture conditions were identified by examining the 3-year rolling average of water storage and identifying periods of relatively stable storage near the median of the simulation. (Typical Period 1 and Typical Period 2 in Attachment 1.)

Across all the periods, the characteristic response of the evapotranspiration cover can be observed; this cover aims to isolate moisture fluctuations to the top of the cover system by using a capillary break between the evaporation zone and the frost protection layer. In both the water balance graphs and the water content graphs, these moisture fluctuations can be observed following precipitation events. For all but the most extreme events, the water content and water storage in the radon barrier layers remain steady, in keeping with the design objectives of the cover. Runoff does not occur at all in this simulation, likely due to the high hydraulic conductivity distribution for the evaporation zone, which was chosen based on the idea of cover naturalization developed in Benson et al. (2011). This is likely conservative with respect to cover performance, as runoff would decrease the storage burden of the evaporation zone during high precipitation events.

The most notable case of increased percolation through the cover can be observed in High Snow Period 1, in which a winter storm event starting around day 443,400 of the simulation causes eventual increased moisture throughout the profile and a sharp increase in percolation. This event is unique in that a period of snow accumulation and snowmelt is followed by another high precipitation event in the form of rain. These two back-to-back precipitation events, combined with the relatively low evapotranspiration values associated with temperatures near freezing, exceed the storage capacity of the evaporation zone, and a long period of higher percolation results. The graphs for Wet Period 1 correspond to the period just after this extreme event. As shown in the water content graph for Wet Period 1, the high moisture conditions in the radon barrier and elevated percolation values persist for several years, while the upper layers of the cover have returned to typical moisture fluctuations.

Less extreme breakthroughs of the capillary barrier can be observed in other periods as well. These include, in decreasing order of severity, High Snow Period 2, High Rain Period 2, and High Rain Period 1. These events can be most easily identified by examining the water content graph for the frost protection layer. Only the event in High Snow Period 2 causes a noticeable increase in percolation over the period. As mentioned above, high precipitation events corresponding to low temperatures are more likely to break through the cover system due to decreased evapotranspiration.

Attachment 1

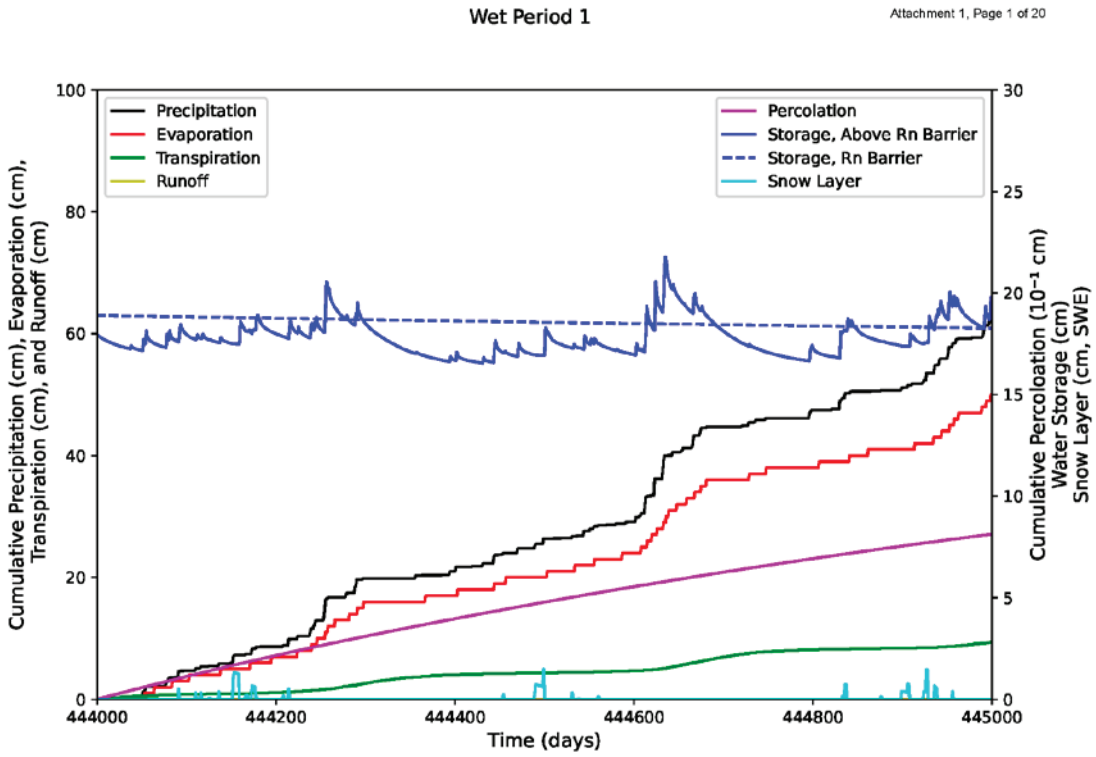

Wet Period 1

Attachment 1, Page 2 of 20

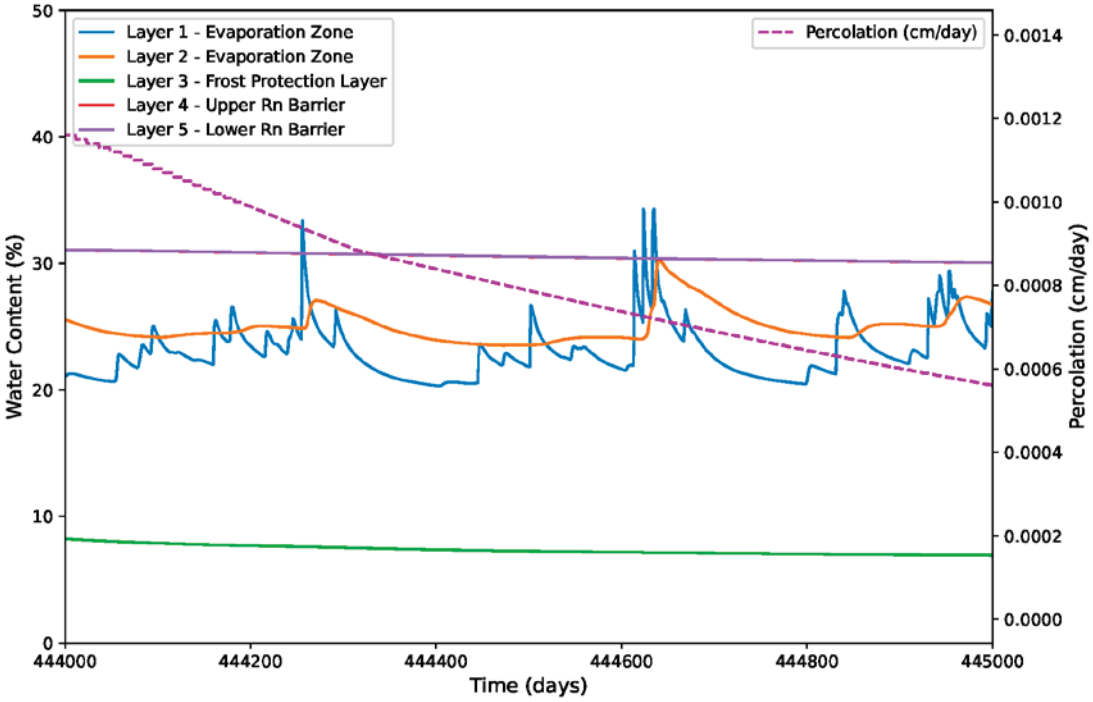

Wet Period 2

Attachment 1, Page 3 of 20

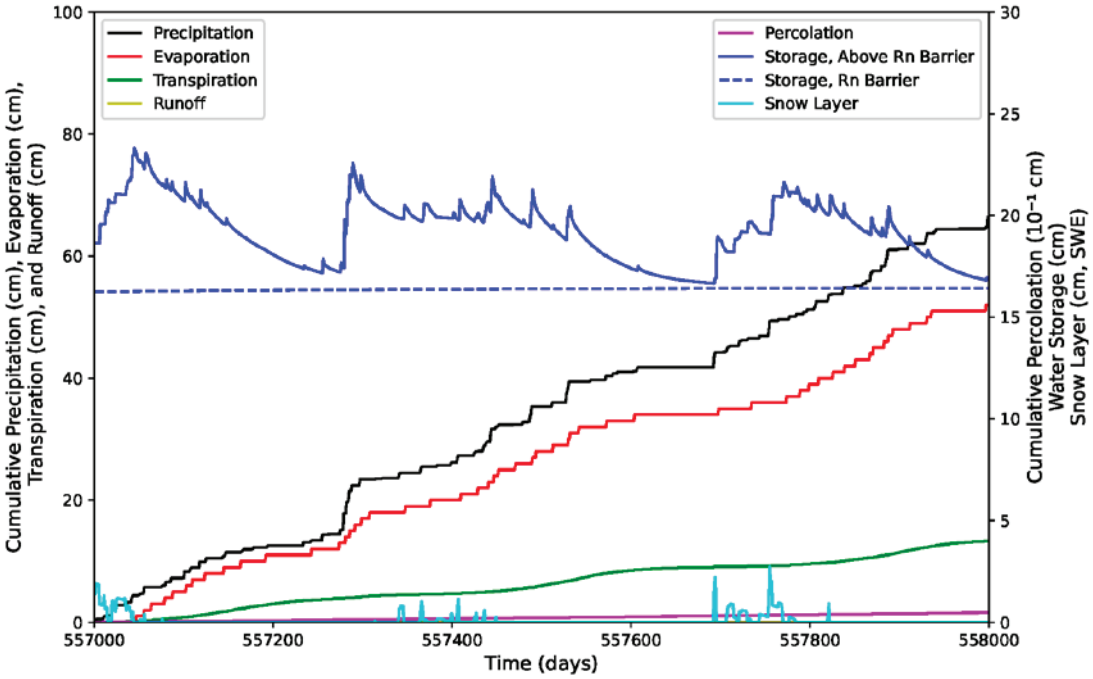

Wet Period 2

Attachment 1, Page 4 of 20

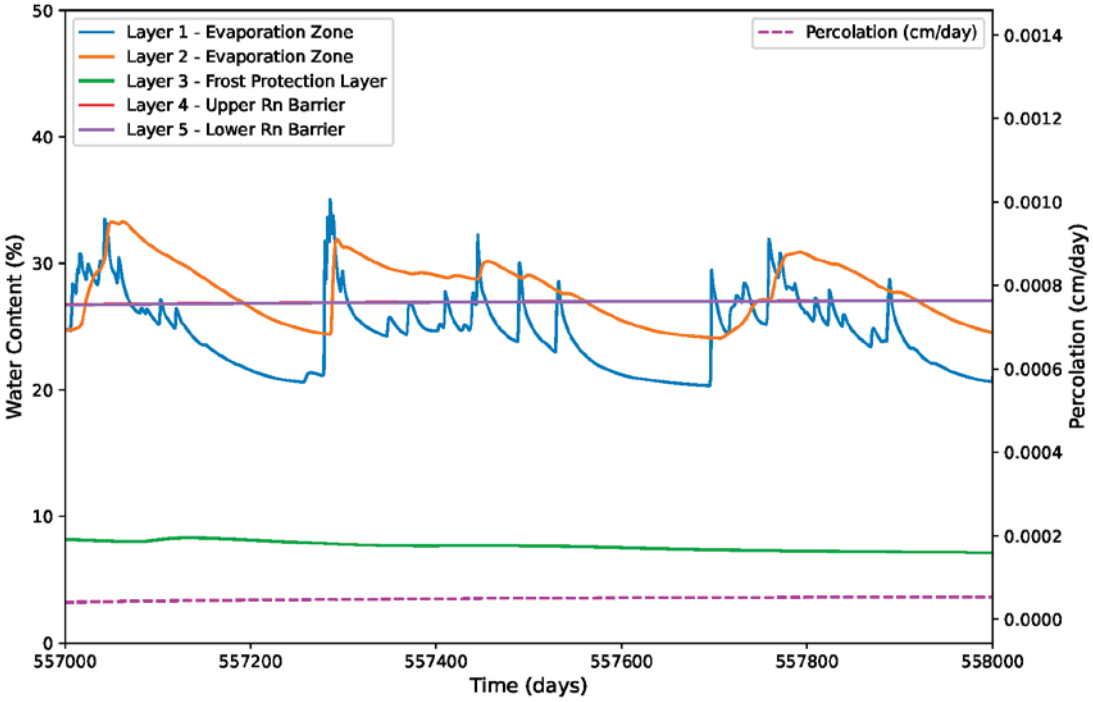

Dry Period 1

Attachment 1, Page 5 of 20

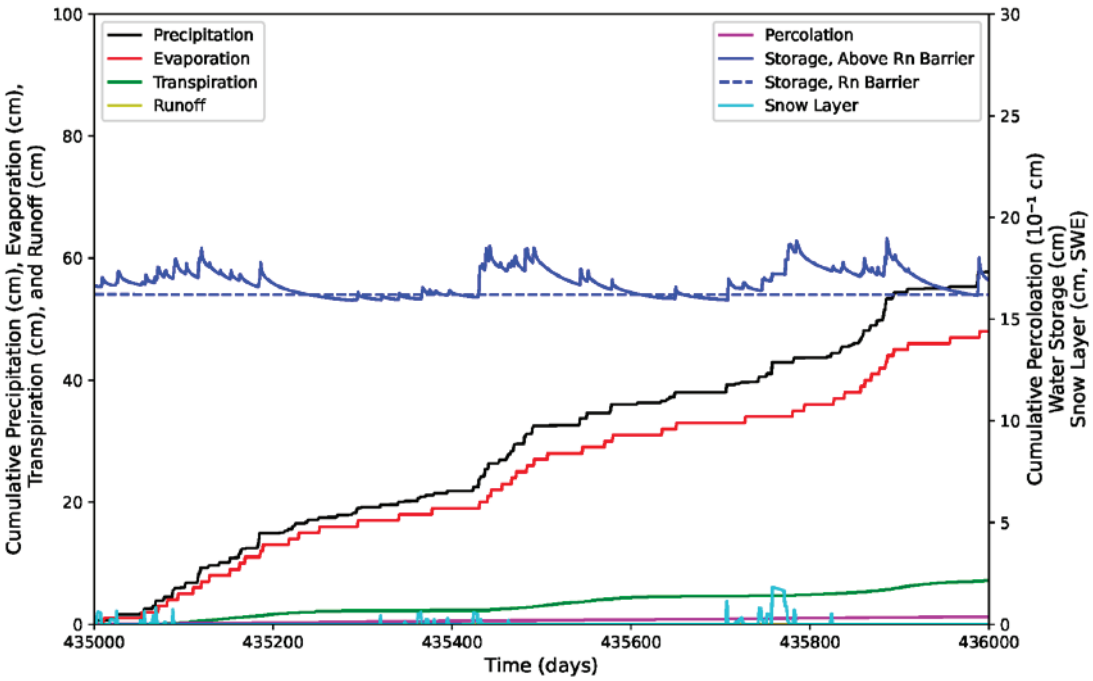

Dry Period 1

Attachment 1, Page 6 of 20

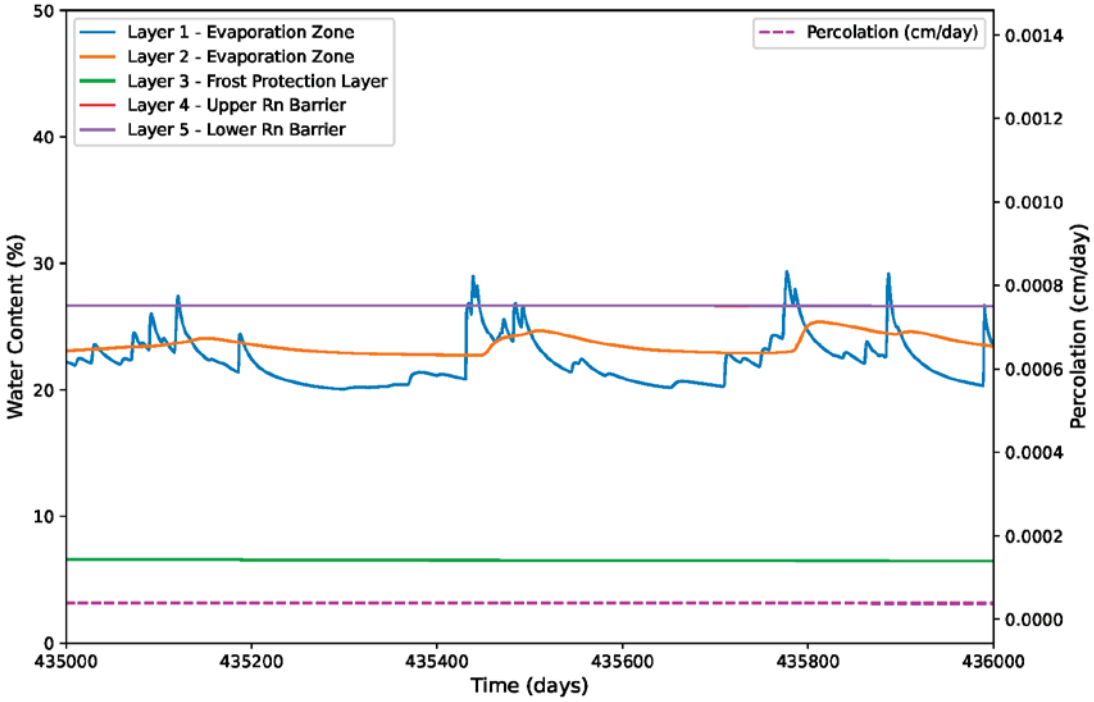

Dry Period 2

Attachment 1, Page 7 of 20

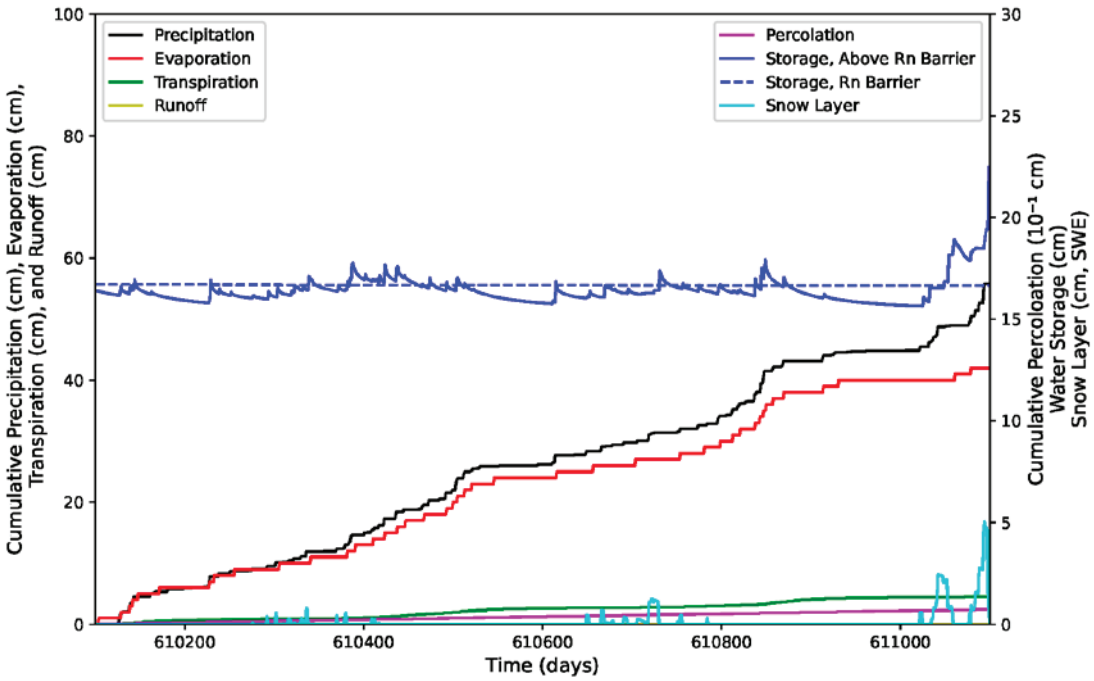

Dry Period 2

Attachment 1, Page 8 of 20

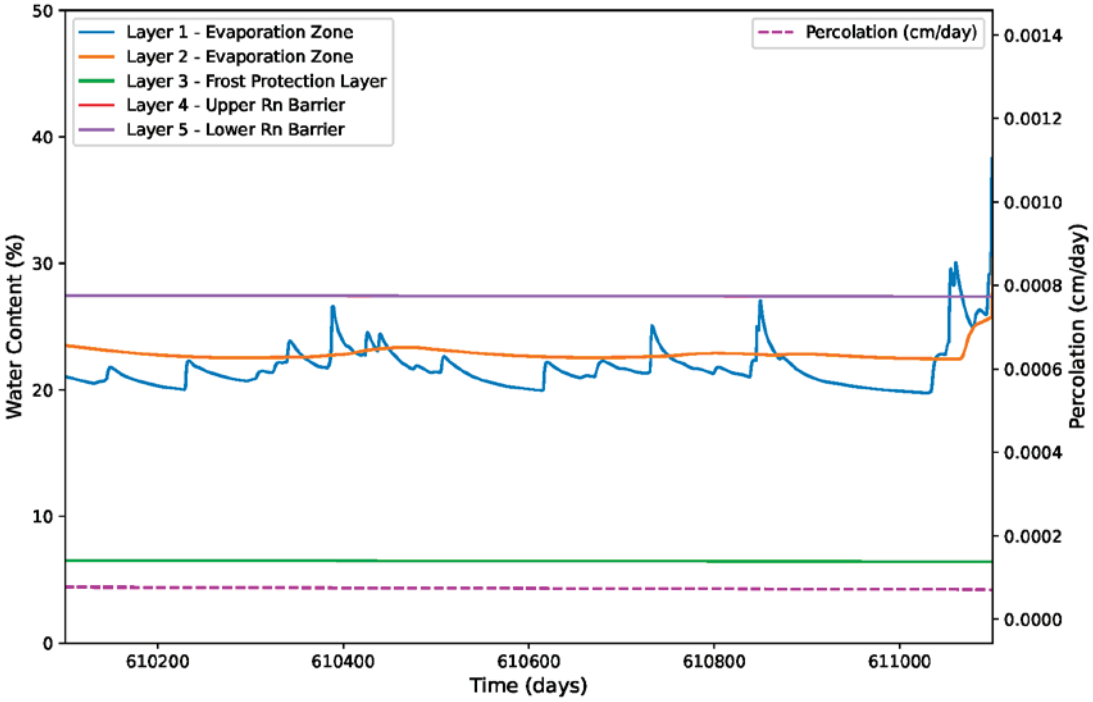

High Rain Period 1

Attachment 1, Page 9 of 20

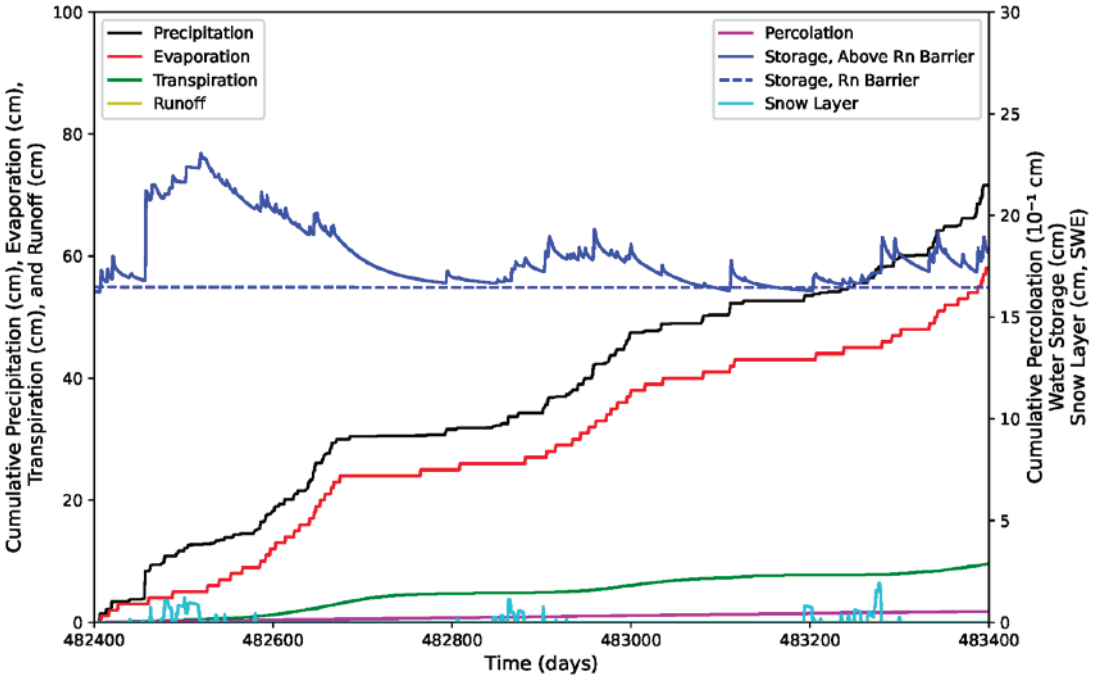

High Rain Period 1

Attachment 1, Page 10 of 20

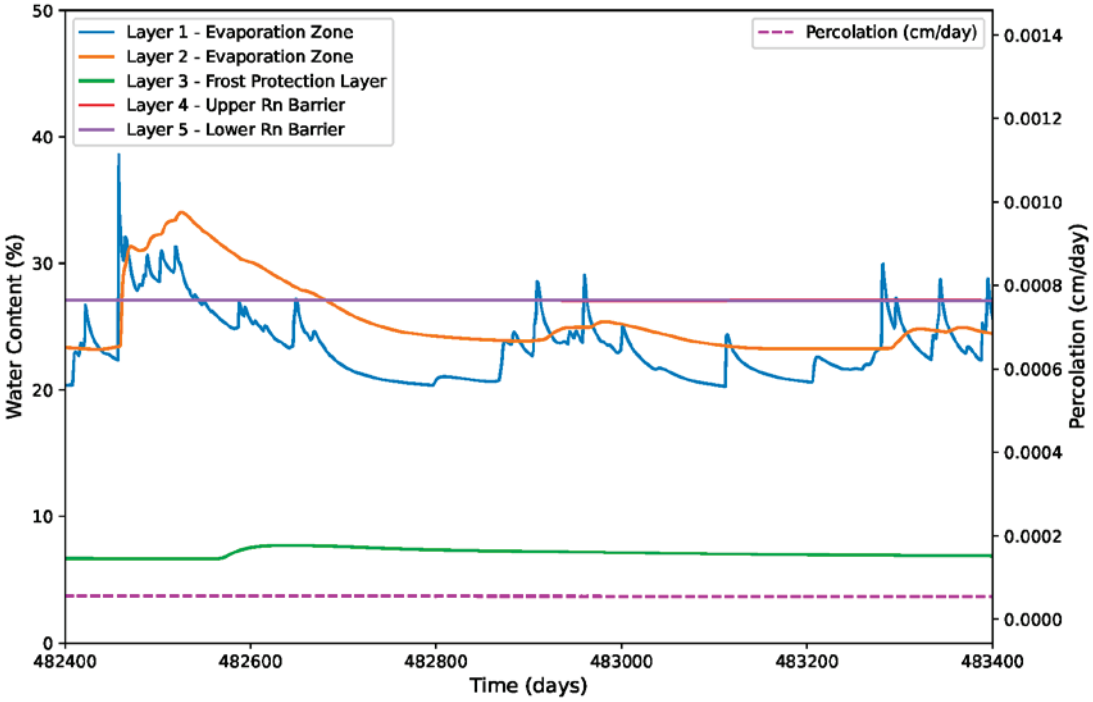

High Rain Period 2

Attachment 1, Page 11 of 20

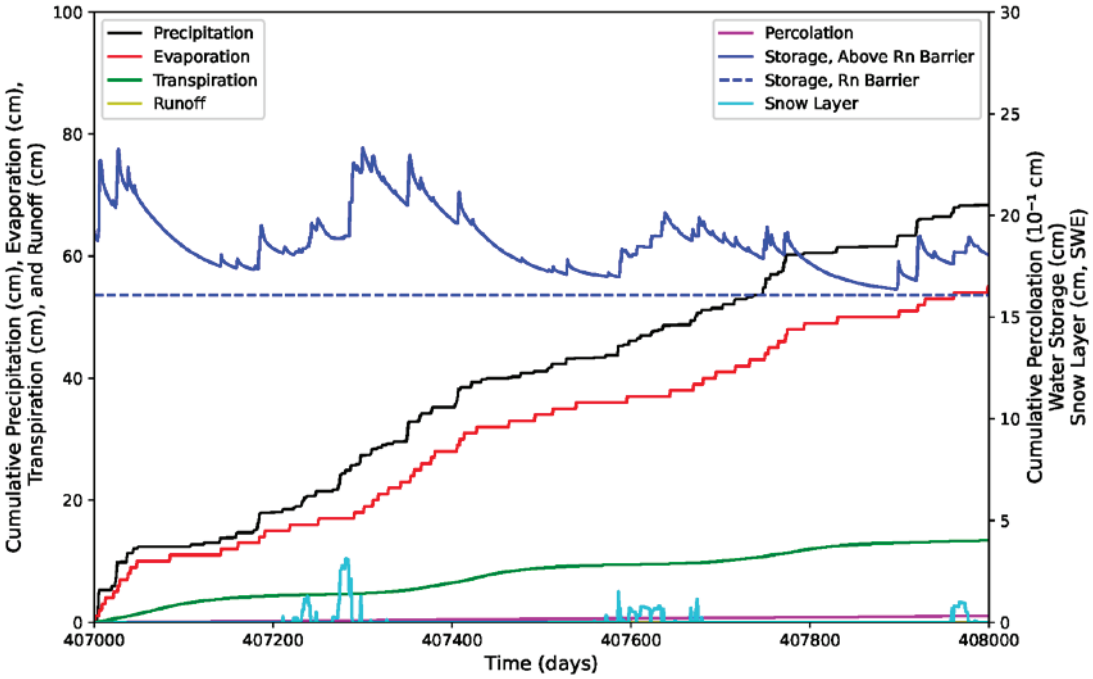

High Rain Period 2

Attachment 1, Page 12 of 20

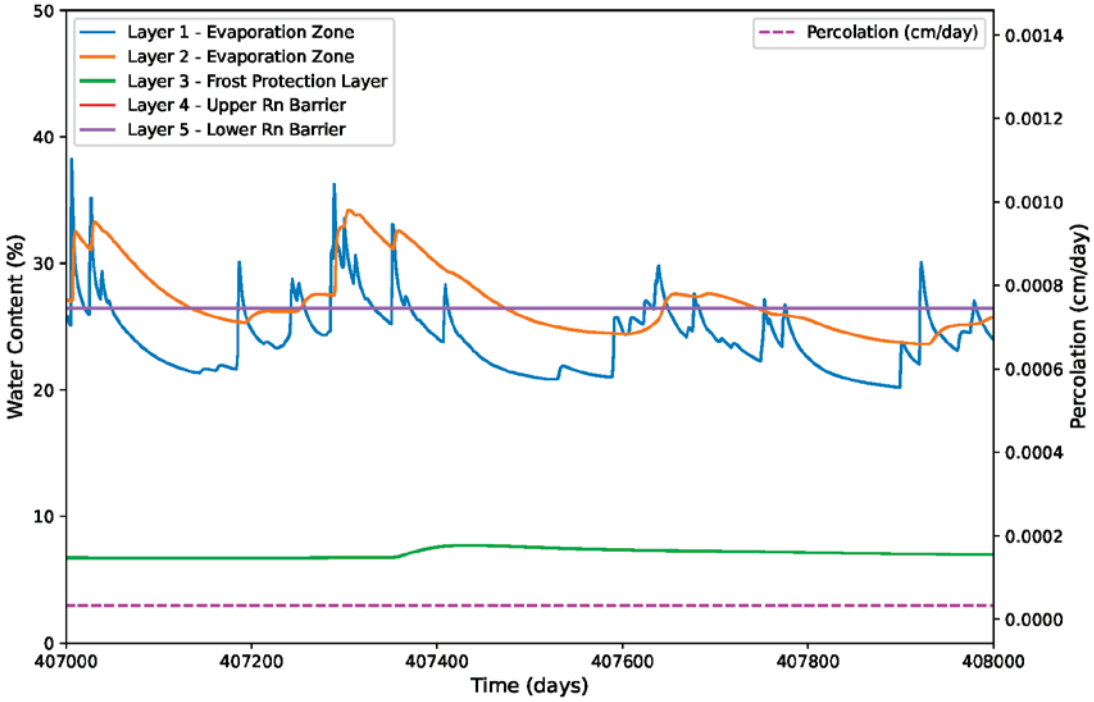

High Snow Period 1

Attachment 1, Page 13 of 20

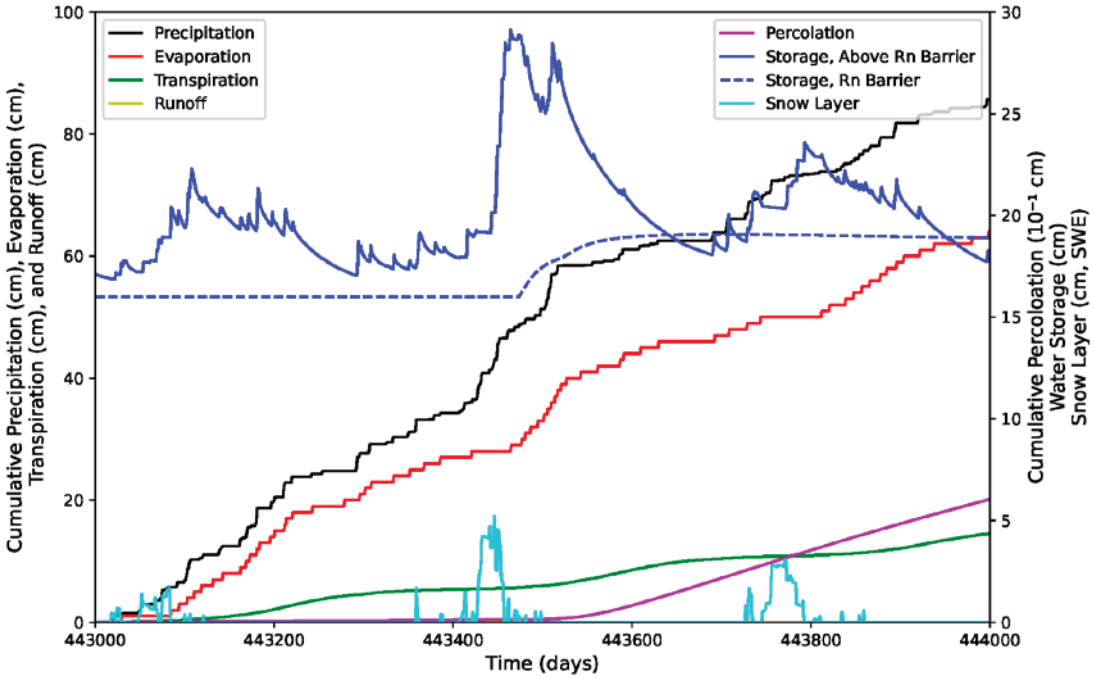

High Snow Period 1

Attachment 1, Page 14 of 20

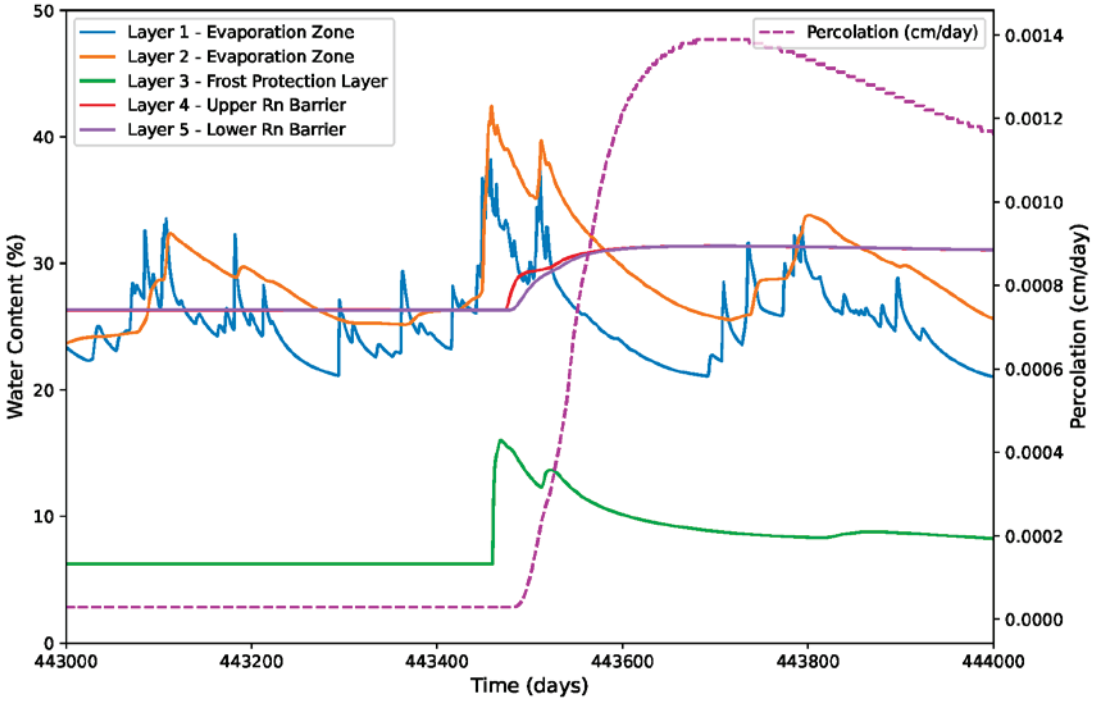

High Snow Period 2

Attachment 1, Page 15 of 20

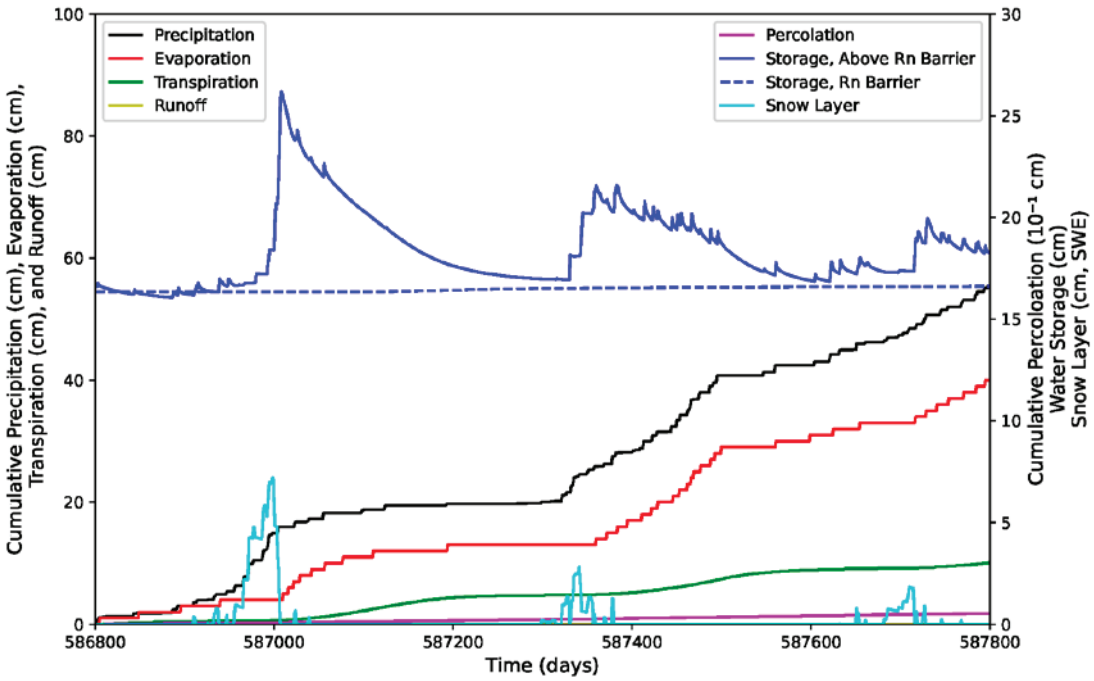

High Snow Period 2

Attachment 1, Page 16 of 20

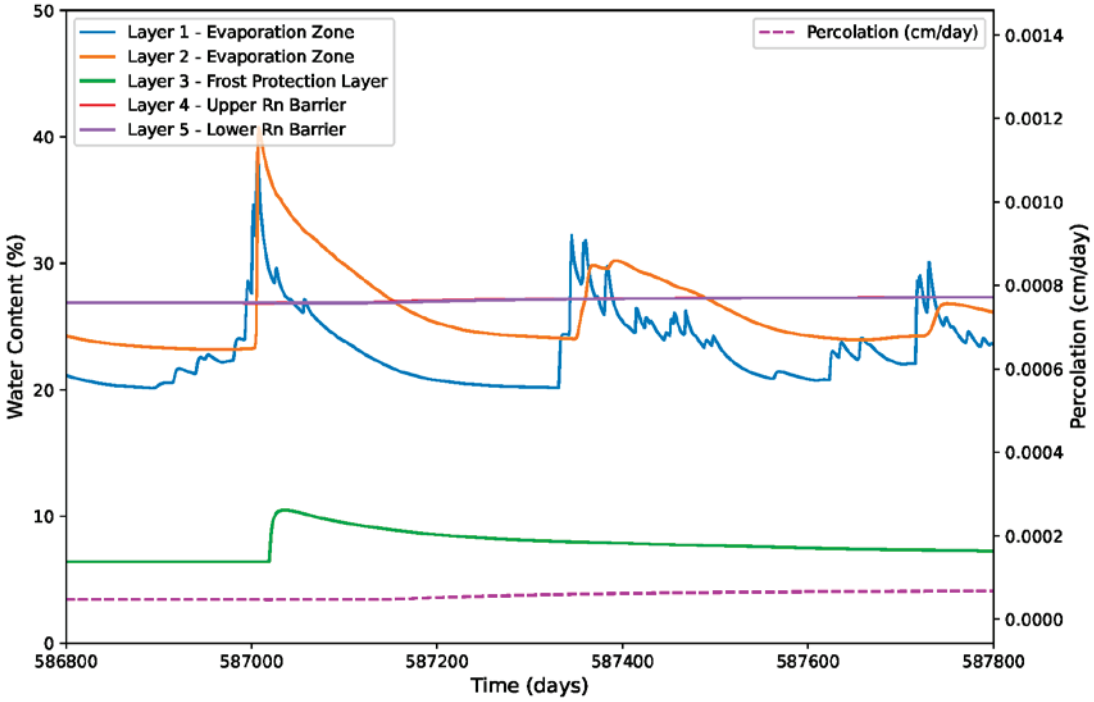

Typical Period 1

Attachment 1, Page 17 of 20

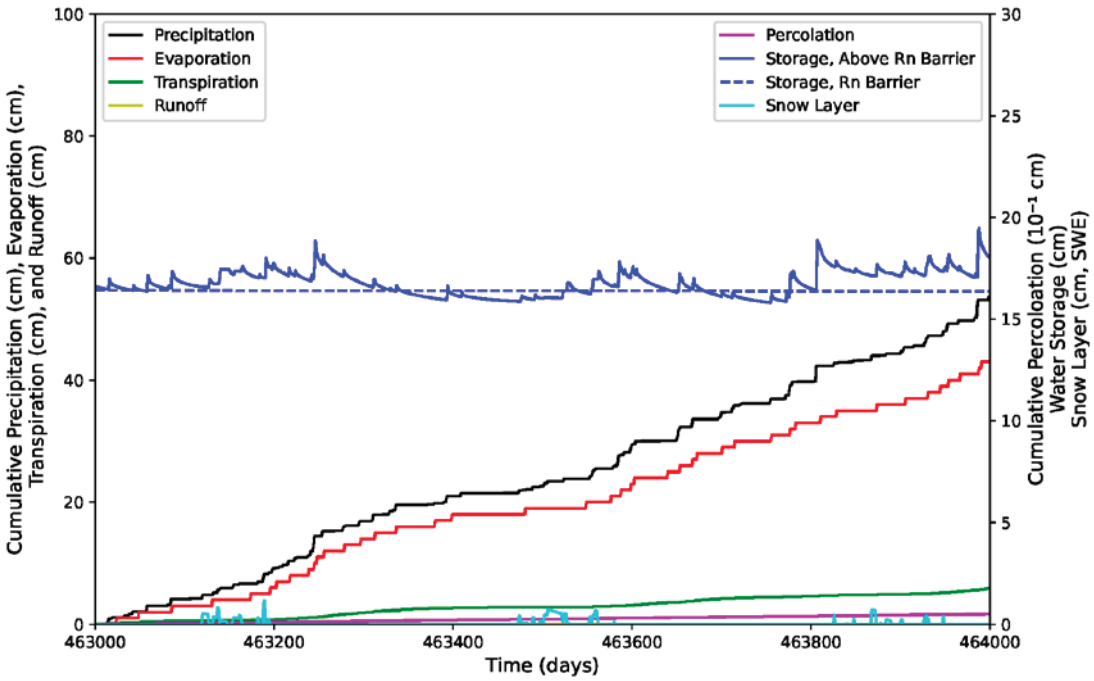

Typical Period 1

Attachment 1, Page 18 of 20

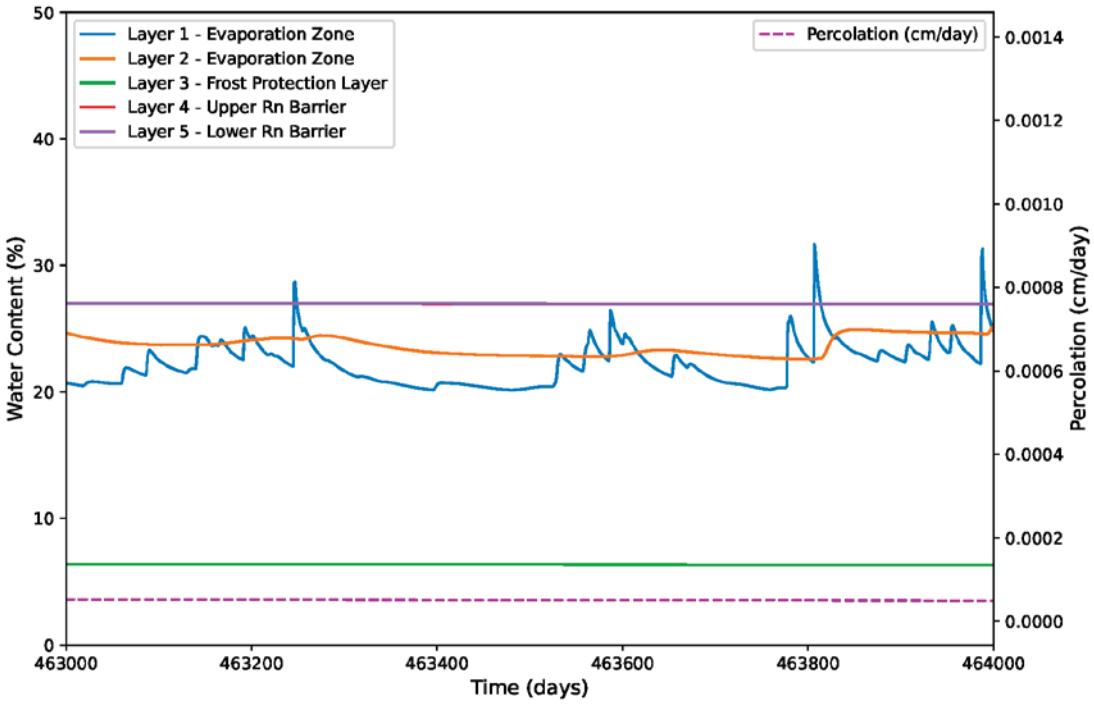

Typical Period 2

Attachment 1, Page 19 of 20

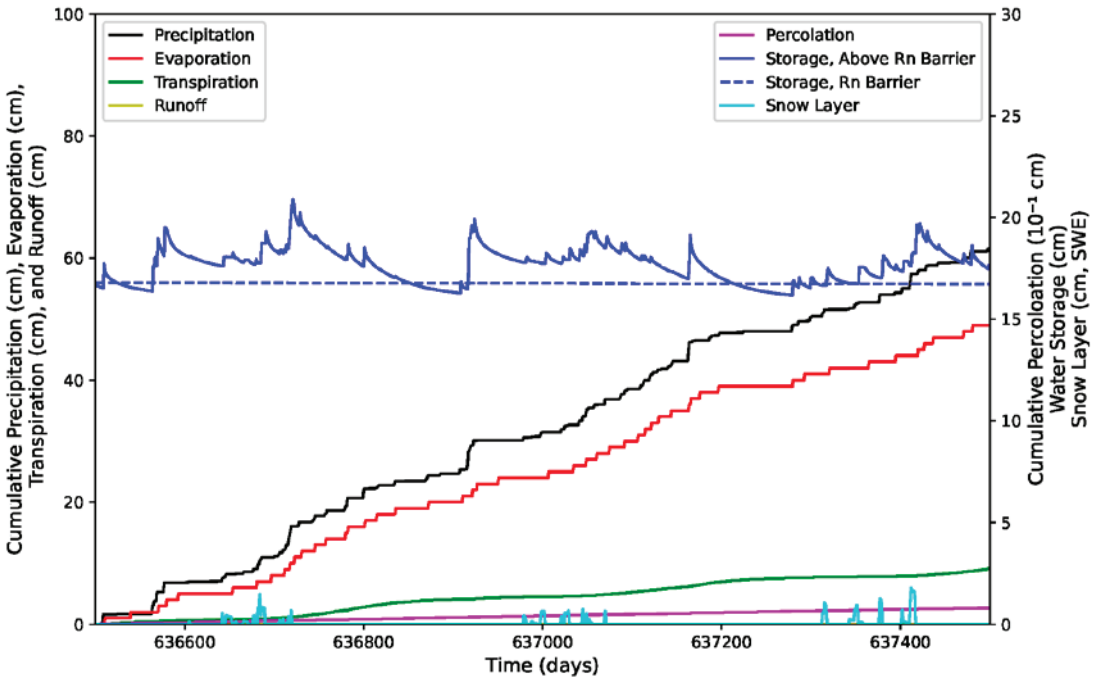

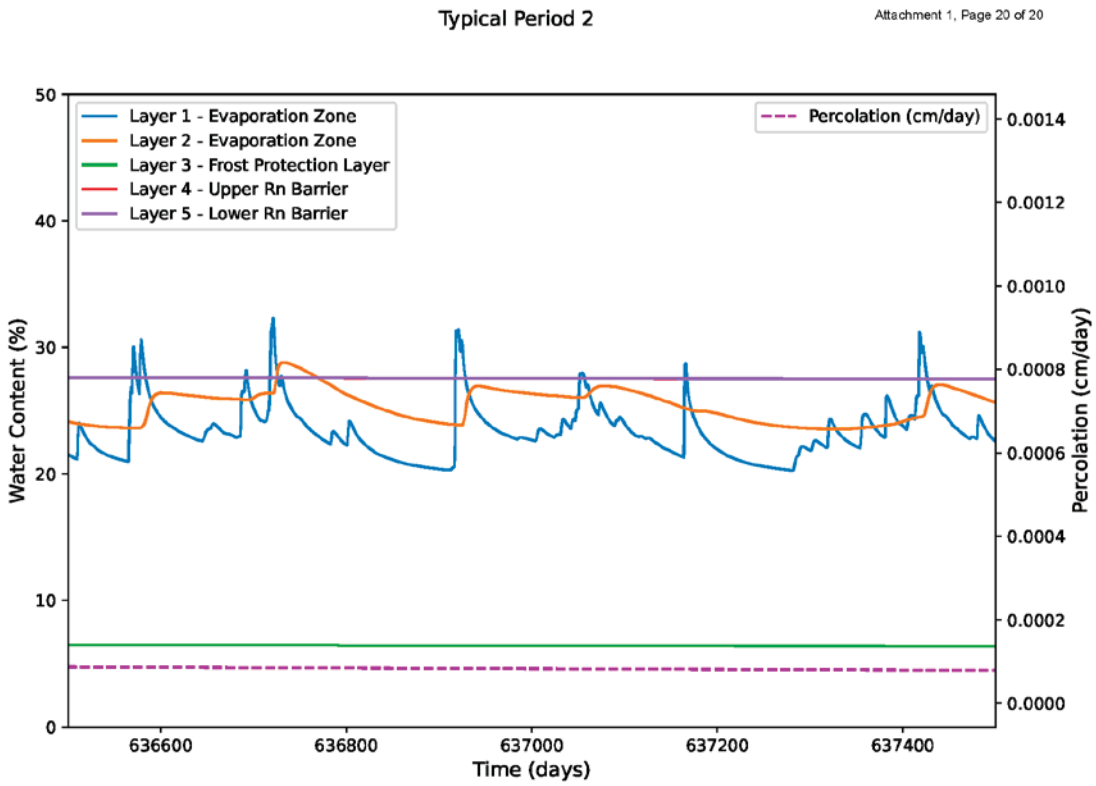

▪ ***O-17***

Efficacy of Capillary Break- The efficacy of the earthen cover is highly dependent on the hydrologic control provided by the capillary break between the evaporative zone and the frost protection layer. Evaluating the sensitivity of the predictions to the assumed conditions is critical to understanding the reliability of the predictions. Provide sensitivity analyses describing how predictions from the variably saturated flow model for the earthen cover varies depending on the sharpness of the capillary break between the evaporative zone and the frost protection layer. For these analyses, systematically vary the unsaturated properties of the frost protection layer over the range anticipated based on the geotechnical and hydraulic properties characterization of the frost protection material. Conduct the analyses over the 1000-yr record and provide the outcomes in terms of water balance graphs and water content graphs like those in RFI question 8.

The requested water balance graphs and water content graphs are provided in the response to RFI O-16 as Attachment 1, immediately above the text of RFI O-17. A brief review of the theory of operation for capillary barrier style ET covers is given below to provide context, and to build a foundation for a mechanistic understanding of the modeled behavior.

Capillary barriers take advantage of differences in soil water characteristic curves (SWCCs) to inhibit downward flow through the cover system. These differences arise from the pore size distribution of the materials in the various cover layers. In ET covers, including the proposed cover at the Clive site, a finer-grained material is typically placed on top of a coarser-grained material, intentionally creating an interface of differing pore sizes. As noted in EPA (2011):

> The discontinuity in pore sizes between the coarser-grained and finer-grained layers forms a capillary break at the interface of the two layers. The break results in the wicking of water into unsaturated pore space in the finer grained soil, which allows the finer grained layer to retain more water than a monolithic cover system of equal thickness.

The purpose of the upper, fine-grained material (known as the evaporation zone in the model) is to maximize the potential for water storage to facilitate its removal by evapotranspiration, while at the same time minimizing the downward flux into the underlying coarse material (known as the FPL in the model). The fine-grained material should also have sufficient permeability to accept precipitation into the soil, to limit other undesirable impacts such as excessive runoff and to allow for plant growth on the surface. The permeability of the material also impacts the rate at which water is redistributed in the fine-grained material due to moisture gradients, which can be important for moving water upward into the evaporative zone after a precipitation event. The goal of the ET cover design is to store all precipitation in the upper fine-grained layer and to make it available for removal upward out of the soil column by ET. If designed properly, and if site conditions allow, no water flows through the coarse material.

A lack of significant flux below the coarse layer, as can be seen in some of the HYDRUS model simulations for the Clive cover, might superficially suggest that the results are insensitive to meteorological conditions, but the results are a product of both meteorology (e.g., potential ET, precipitation amount and pattern) and the cover design. The key questions addressed below are: 1) Under what circumstances can the evaporative zone material store and release the incoming precipitation while limiting flow to the underlying coarse material, thereby making flows in the lower cover seemingly unresponsive to precipitation? 2) Can this be explained mechanistically using the principles of unsaturated flow? 3) What are the critical material properties governing these mechanisms?

The mechanics of this interaction are best understood by examining the SWCCs of the materials involved, which govern water content and hydraulic conductivity as a function of pressure head (tension). As an example, the SWCCs and properties discussed below are taken from the DU PA v1.4 HYDRUS model simulation that produced the highest percolation through the cover (simulation #20 of 50). However, the analysis can and will be applied to a variety of parameter sets as requested by the RFI.

Under unsaturated conditions, a coarse material that lacks a significant fraction of fine pores will not imbibe water under high water tension (negative pressure head, h) because of the small capillary forces associated with a larger pore structure. Large pores cannot hold water or support flow at high tensions because capillary forces vary as the inverse of pore radius, which implies that large pores are empty at high tension. Figure 13 shows the SWCC for the FPL as implemented in the DU PA v1.4 HYDRUS model, which used the van Genuchten model with α and n equal to 7.5 m-1 and 1.89, respectively. Under normal circumstances, this material will be quite dry in a semi-arid environment as the specific retention (i.e., the water content under only gravity drainage) is quite low. Specific retention can be approximated as the water content at a tension of 3 m (Stephens 1996), which equates to a water content only about 0.02 above the irreducible water content (θ_r) for this material.

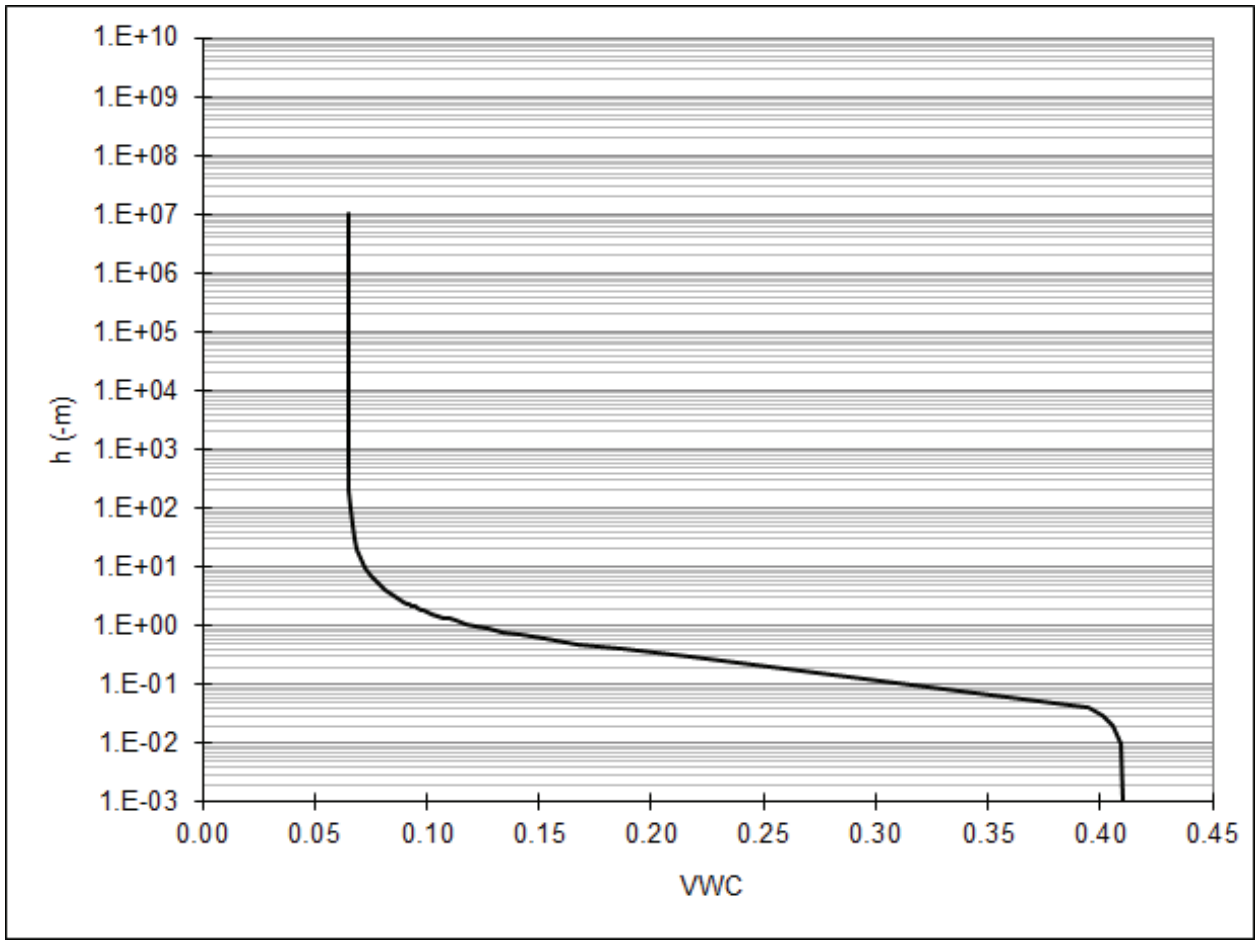

Figure 13. SWCC for the FPL as modeled in DU PA v1.4.

For this material, at higher tensions (*h*), even large changes in tension result in very small changes in volumetric water content. For example, an order of magnitude change in tension from 100 m to 10 m is associated with a change of water content from 0.066 to 0.072 for the SWCC shown in Figure 13. As stated above, this is due to the lack of small pore sizes in the material.

The importance of prevailing tensions in the system is also reflected in the unsaturated hydraulic conductivity function for the materials, as shown in Figure 14. Though a coarse material typically has a high hydraulic conductivity under saturated conditions (K_{sat}), under high tension unsaturated conditions the conductivity can be very low. The modeled frost protection layer, for example, has a K_{sat} of over 100 cm/day, but at a tension of 10 m the conductivity is virtually zero (~3E-7 cm/day). Unsaturated conductivity vs. pressure head is shown in Figure 14 for the FPL and the evaporation zone as simulated in the same high percolation model simulation #20.

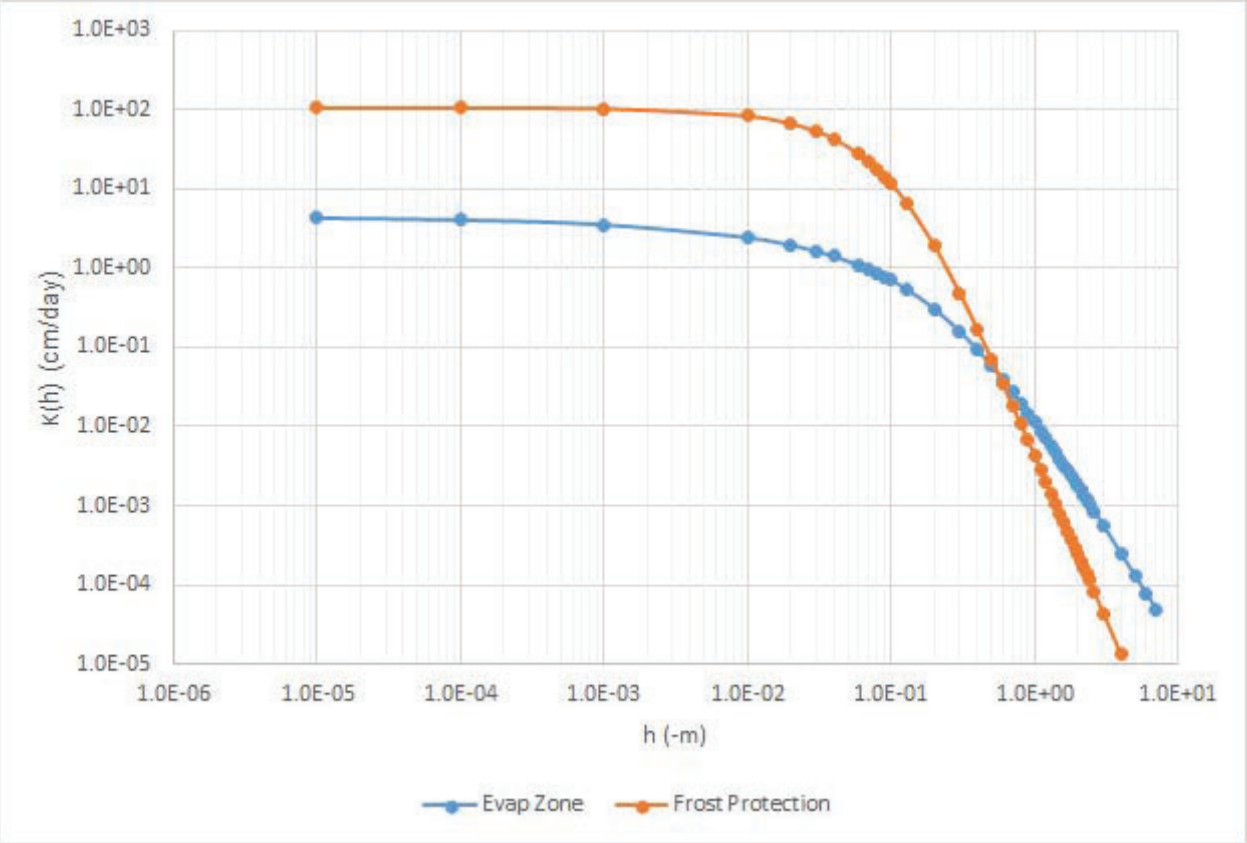

Figure 14. Unsaturated conductivity as a function of pressure head for a coarse and fine material.

Note that the conductivity for the evaporation layer exceeds that of the FPL in the high-tension regime down to pressure heads of about -0.6 m, despite the fact that the K_{sat} of the FPL is nearly two orders of magnitude greater than that of the evaporation zone.

At lower tensions, the larger pores in a coarse material can become saturated, and as a result the water content and conductivity increase markedly. As can be seen in Figure 13, the SWCC bends sharply at around tensions of 2 m to 10 m. An order of magnitude change in tension in this range, for example from 3 m to 0.3 m, would result in a water content change from 0.087 to 0.218, while the conductivity would change four orders of magnitude from about 4.5E-5 cm/day to 4.9E-1 cm/day. The dramatic increase in conductivity is due to the fact that frictional forces vary inversely with the fourth power of the pore radius.

Thus, the range of tensions maintained in the FPL and at the interface with the evaporation zone will be of critical importance to the flow through it, as lower tensions would engage larger pores in flow and storage. Water coming downward through the cover would have to generate a large enough pressure pulse to overcome the difference in capillary forces between the fine and coarse layers in order to fully penetrate the cover system. Stephens (1996) summarized this effect as follows:

> Owing to heterogeneity, the downward percolation of water or redistribution may virtually cease where the infiltrated water migrating through a fine soil encounters a dry and relatively uniform, coarse textured layer. This occurs when the pressure head in the water pulse is not sufficiently great to force water to enter the large pores of the coarse soil.

This can also be observed through the lens of specific moisture capacity, which is defined as the first derivative of the SWCC with respect to pressure head ($d\theta/dh$), and is interpreted as the volume of water released or taken into storage per unit change in pressure head. The specific moisture capacity for the FPL is shown in Figure 15. Note that, for tensions above about 2.5 m, the specific moisture capacity is essentially zero, meaning that little water is taken or released from storage despite potentially large changes in pressure. The value of the pressure head associated with this threshold depends, of course, on the SWCC for the material. However, any coarse material suitable for a capillary barrier will have similar-shaped SWCC and specific moisture capacity.

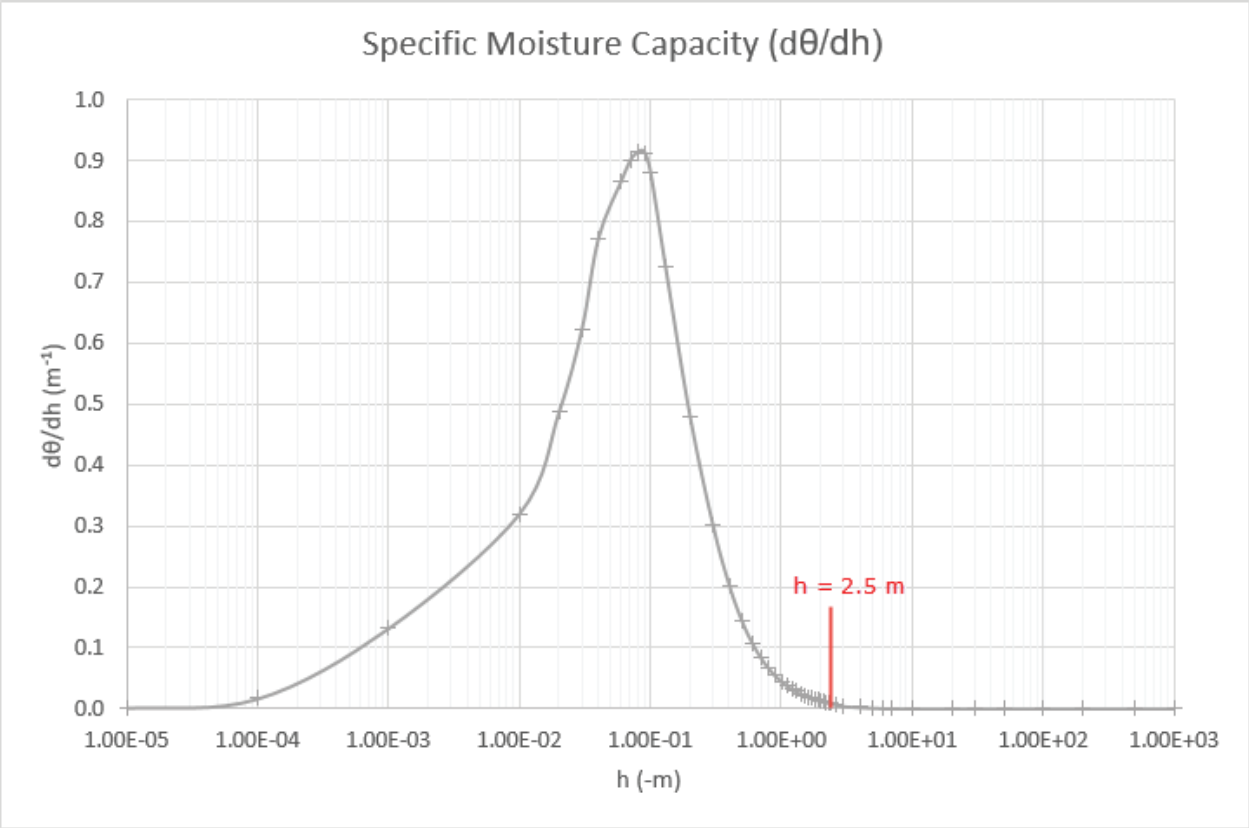

Figure 15. Specific moisture capacity for the FPL as modeled in DU PA v1.4.

The cover performance thus hinges on whether the evaporative zone can store and release the incoming precipitation while maintaining sufficiently high tensions such that the coarse material cannot store or conduct a significant amount of water. If tension deviations occur at significantly higher values (i.e., to the right side of the specific moisture capacity curve in Figure 15), then one should expect the flow through the FPL and below to be insensitive.

Figure 16 shows this behavior in the model output for simulation #20. Fifty years are shown, including a notably wet period beginning at around model year 890. The tension at the interface of the evaporative zone and FPL (green curve) is constantly changing as water is moved in and out of the model domain via precipitation and evapotranspiration. The flux through the FPL (blue curve) is insensitive to most of the oscillations, except when the tension dips to around 250 cm or below (red line). For those periods, a response is seen in the flow through the frost protection layer, as predicted by examination of Figure 15. At around model year 890, there are two significant drops in tension, with the second drop down to around 100 cm. This produces the most significant downward flux in the period shown.

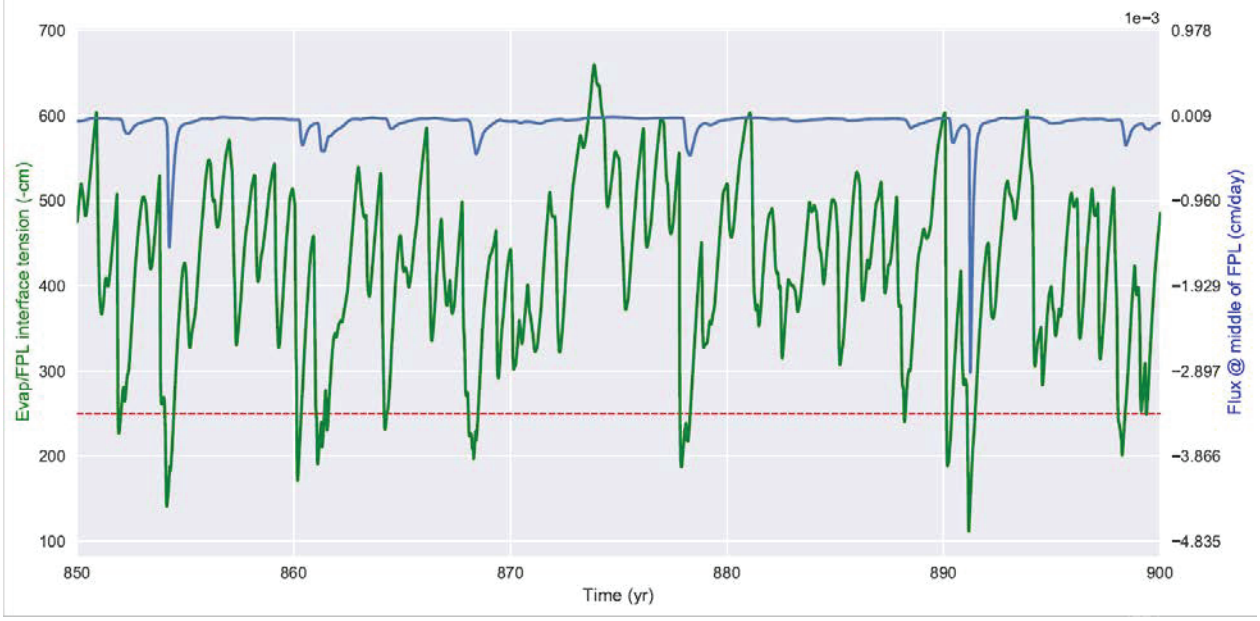

Figure 16. Evaporation zone pressure head and flux through the FPL vs. time for a wet period in simulation #20. The red dotted line is drawn at a pressure head of -250 cm. Flux values are negative for downward flow.

While the above discussion focuses on the SWCC for the coarse frost protection layer, the SWCC of the finer evaporation zone material also warrants discussion. In fact, the regression model in the DU PA v1.4 reflects that percolation is sensitive to the SWCC parameters in the evaporation zone. This can be understood in the context of the threshold effect described above for the coarse layer.

For the cover to perform effectively as a capillary barrier, the evaporation zone needs to store and release infiltrated water while maintaining a range of pressure heads that preclude flow in the underlying frost protection layer. Performance can thus be estimated by evaluating how much water can be stored in the evaporative zone while keeping tensions below this critical range. Figure 17 shows the SWCC for the FPL along with the evaporation zone layer for two different simulations from the DU PA v1.4 modeling.

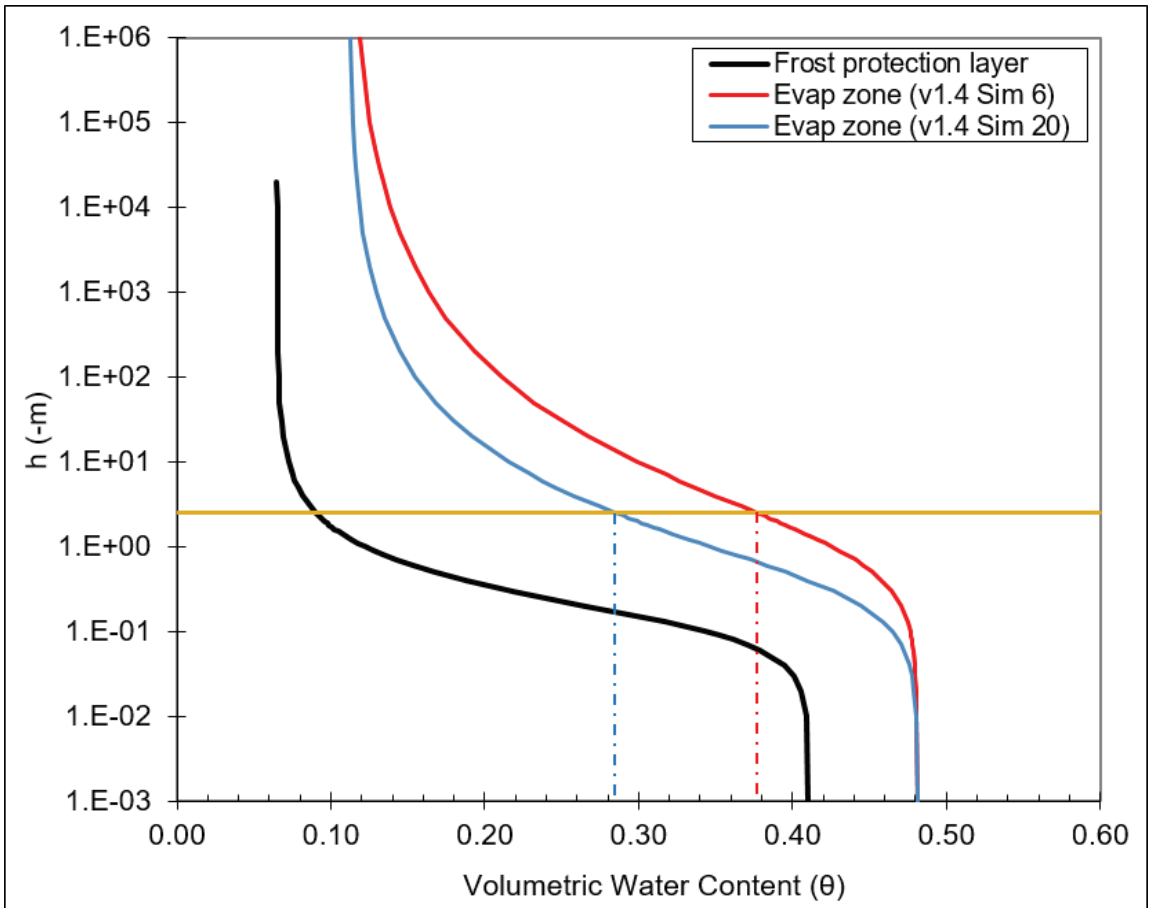

Figure 17. SWCCs for the FPL and two realizations of the evaporation zone layer. The tan horizontal line is drawn at a tension of 250 cm, while the dotted lines indicate the corresponding water content for the evaporative zone curves.

Examination of Figure 17 shows that, at a tension of 250 cm, the volumetric water content of the evaporation zone in simulation #6 (red) would be at around 38%, while the water content for the evaporation zone in simulation #20 (blue) would be around 28%. Viewed through this lens, it is not surprising that the resulting percolation in simulation #6 was much lower than in simulation #20 (7.9E-3 mm/yr and 1.8E-1 mm/yr, respectively), as the evaporation zone in simulation #6 can store much more water before significant breakthrough of the FPL occurs. This is precisely the effect mentioned in the RFI as the "sharpness of the break" in material properties.

The 50 simulations performed to support DU PA v1.4 each had a different SWCC for the evaporation zone, and thus comprise a systematic set of simulations that vary the sharpness of the material contrast at this interface. The regression equations for percolation and water content incorporate these relationships. The parameters of the van Genuchten SWCC model are θ_s, θ_r, α, and n. The first two specify the saturated and residual water contents, respectively, which define the endpoints at either end of the SWCC as shown in Figure 17. The remaining parameters define

the shape of the intervening curve. Alpha can be simply interpreted as inversely proportional to the pressure head at which the inflection point on the right side of Figure 17 occurs, commonly known as the air entry pressure head. Simulation #20 has a higher α (0.028 1/cm) than simulation #6 (0.011 1/cm), and, therefore, a lower air entry pressure. The *n* parameter is related to the grain size distribution and can be simply interpreted as inversely related to the slope of the central portion of the SWCC. For example, the FPL has the highest *n* value in Figure 17 (1.89, vs. 1.28 and 1.38 for simulations #6 and #20, respectively) and, therefore, the least steep slope in the central portion of the curves pictured.

With these relationships in mind, close examination of Figure 17 would predict that the best performing evaporative zone materials should have low α and low *n*, as these properties would be most conducive to water storage while maintaining relatively high pressure heads (i.e., pushing the evaporation zone curves up and to the right in Figure 17). Conversely, based on Figure 17, poor performance would be associated with high α and high *n*. These relationships manifest in exactly this fashion in the regression equations of DU PA v1.4, which associate higher α and higher *n* in the evaporation zone with increased percolation. These relationships would be reversed, of course, when discussing the properties of the FPL, in which high α and high *n* are desirable for limiting percolation.

In summary, a mechanistic explanation for the capillary barrier performance is presented based on the theory of unsaturated flow. Insensitivity of conditions in the lower portion of the cover to meteorological forcing is the expected and intended behavior in such a cover design, as the evaporative zone stores and releases water while maintaining a pressure regime in which the coarse underlying materials do not allow flow. An example of the predicted behavior in the model output was presented. The sensitivity of the sharpness of the material contrast was evaluated in the 50 simulations performed for DU PA v1.4. The relationships predicted by the regression equations comport with the predictions of the analysis of the system dynamics based on first principles of unsaturated flow. As suggested by the RFI, the material contrast is fundamental to the performance of the cover system.

▪ ***O-18***

Impacts of Bioturbation from Burrowing Mammals- SWCA (2012) indicates that the Federal Cell is within a habitat associated with badgers, burrowing owls, and ants. SWCA (2012) indicates that a biointrusion barrier will be needed for earthen covers at the Clive site to address badgers and owls. Williams et al. (2022) illustrate how ant colonization can alter the hydraulic properties of protection layers and radon barriers. Describe how biointrusion, bioturbation and other disturbance of the cover associated with burrowing mammals, birds, and insects will affect the hydraulic properties of the cover soils, the efficacy of the capillary break, and percolation. Document the scientific basis underpinning the impacts from biointrusion and bioturbation that are described.

- ***SWCA, 2012, Vegetated Cover System for the Energy Solutions Clive Site: Literature Review, Evaluation of Existing Data, and Field Studies Summary Report; Prepared for EnergySolutions by SWCA Environmental Consultants, Salt Lake City UT, August 2012.***
- ***Williams, M., Fuhrmann, M., Stefani, N., Michaud, A., Likos, W., Benson, C., and Waugh, W., 2022, Evaluation of In-Service Radon Barriers over Uranium Mill Tailings Disposal Facilities: NUREG/CR-7288, Office of Research, US Nuclear Reg. Comm., Washington, DC***

Biological organisms play an important role in soil mixing processes, and therefore are potentially important mediators of transport of buried wastes from deeper layers to shallower layers or the soil surface. Three broad categories are evaluated for their potential effect on the redistribution of radionuclides at the Clive facility: plants, ants, and burrowing mammals. The impact of these flora and fauna will be limited largely to the top several meters, based on the depth of their roots and burrows. Details for all three categories can be found in Sections 3.0, 4.0, and 5.0 respectively of the *Biological Modeling* white paper (Neptune 2021a). In DU PA v2.0, these impacts are explicitly modeled for their potential to bring contamination from depth to the cell surface.

Bioturbation of cover soils is anticipated in localized areas. SWCA (2012), Table 6 estimates the total number of ant mounds and the total mound area per plot for nine field study plots at the Clive site and local analogs. A total of 9.6 m^2 of ant mound area is reported for a study area totaling 9000 m^2, or an impact of slightly more than 0.1%.

The effects of bioturbation on hydraulic performance were not explicitly modeled in terms of potential impact to the hydraulic properties of the Federal Cell cover system. However, a broad distribution for the saturated hydraulic conductivity (K_s) of the radon barriers is used for unsaturated zone modeling. This broad distribution provides some qualitative accounting for the effects of bioturbation. The K_s values for the radon barrier layers were sampled from a distribution developed from a minimum value of 4.32×10^{-3} cm/day corresponding to the design specification for the upper radon barrier (Energy*Solutions* 2021b), and 1st, 50th, and 99th percentile values of 0.65 cm/day, 3.8 cm/day, and 52 cm/day, respectively, which are from a range of in-service ("naturalized") clay barrier K_s values described by Benson et al. (2011), Section 6.4, p. 6-12. A shifted lognormal distribution was fit to the 1st, 50th, and 99th percentiles, and the minimum value of 4.32E-3 cm/day was used as a shift. The resulting distribution is:

$Ks \sim Lognormal(geom.mean: 3.37\ cm/day, geom.sd: 3.23\ cm/day)$, with a right shift of 0.00432 cm/day

For all HYDRUS simulations, the same K_s value was applied to both the radon barriers (layers 4 and 5) as well as the surface and evaporative zone layers (layers 1 and 2) in order to understand variations of the output due to K_s variation of the Unit 4 derived materials given a long-term naturalized condition. This distribution was sampled to provide a unique value for all 1000 simulations.

By including a range of in-service hydraulic permeability values up to five orders of magnitude above the construction specification, potential localized effects of bioturbation are bounded.

References

Anderson, M.P., et al., 2015. *Applied Groundwater Modeling: Simulation of Flow and Advective Transport, 2nd edition*, Academic Press, London

Arora, B., et al., 2019. Understanding and Predicting Vadose Zone Processes, *Reviews in Mineralogy & Geochemistry* 85 (2019) 303–328

Benson, C.H., 2021. Facilitating Informed Decision-Making for Waste Containment Systems, proceedings of the *Waste Management Symposia 2021, March 7–11*, Phoenix AZ, 2021

Benson, C.H., et al., 2011. *Engineered Covers for Waste Containment: Changes in Engineering Properties and Implications for Long-Term Performance Assessment,* NUREG/CR-7028, Volume 1, United States Nuclear Regulatory Commission, Washington DC, December 2011

Beven, K., and P. Germann, 1982. Macropores and Water Flow in Soils, *Water Resources Research* 18 (5) 1311–1325

Bingham Environmental, 1991. *Hydrogeologic Report, Envirocare Waste Disposal Facility, South Clive, Utah,* prepared for Envirocare of Utah, Bingham Environmental Inc., Salt Lake City UT, October 1991

Bjornstad, B.N., and S.S. Teel, 1993. *Natural Analog Study of Engineered Protective Barriers at the Hanford Site,* PNL-8840, UC-510, prepared for United States Department of Energy, Pacific Northwest Laboratory, Richland WA, September 1993

Black, P., et al., 2019. Scaling Input Distributions for Probabilistic Models - 19472, proceedings of the *Waste Management Symposia 2019, March 3-7*, Phoenix AZ, 2019

Blöschl, G., and M. Sivapalan, 1995. Scale Issues in Hydrological Modelling: A Review, *Hydrological Processes* 9 (1995) 251–290

Bradley, B.A., and J.F. Mustard, 2005. Identifying Land Cover Variability Distinct from Land Cover Change: Cheatgrass in the Great Basin, *Remote Sensing of Environment* 94 (2005) 204–213 doi: 10.1016/j.rse.2004.08.016

Bylo, L.N., et al., 2014. Grazing Intensity Influences Ground Squirrel and American Badger Habitat Use in Mixed-Grass Prairies, *Rangeland Ecology and Management* 67 (2014) 247–254 doi: 10.1016/j.rama.2016.07.001

Camacho-De Coca, F., et al., 2004. Vegetation Cover Seasonal Changes Assessment from TM Imagery in a Semi-Arid Landscape, *International Journal of Remote Sensing* 25 (17) 3451–3476 doi: 10.1080/01431160310001618761

Carsel, R.F., and R.S. Parrish, 1988. Developing Joint Probability Distributions of Soil Water Retention Characteristics, *Water Resources Research* 24 (5) 755–769

Chari, M.M., et al., 2020. Modelling Soil Water Infiltration Variability Using Scaling, *Biosystems Engineering* 196 (2020) 56–66 doi: 10.1016/j.biosystemseng.2020.05.014

Christensen, J.H., et al., 1996. *The HIRHAM4 Regional Atmospheric Climate Model,* Scientific Report 96-4, Danish Meteorological Institute (DMI), Copenhagen, Denmark, 1996

Dagan, G., 1989. *Flow and Transport in Porous Formations: A Theoretical Approach*, Springer-Verlag, Berlin

de Rooij, G.H., 2011. Averaged Water Potentials in Soil Water and Groundwater, and Their Connection to Menisci in Soil Pores, Field-Scale Flow Phenomena, and Simple Groundwater Flows, *Hydrology and Earth System Sciences* 15 (2011) 1601–1614 doi: 10.5194/hess-15-1601-2011

Diffenbaugh, N.S., and F. Giorgi, 2012. Climate Change Hotspots in the CMIP5 Global Climate Model Ensemble, *Climate Change* 114 (3–4) 813–822 doi: 10.1007/s10584-012-0570-x

Dobre, R.G., et al., 2017. *Snowmelt Infiltration Using Hydrus-1D Based on a Snow Surface Energy Balance Model for Bucegi Mountains, Romania*, available from https://www.sgem.org/index.php/elibrary-research-areas?view=publication&task=show&id=3455

Elmore, A.J., et al., 2003. Regional Patterns of Plant Community Response to Changes in Water: Owens Valley, California, *Ecological Applications* 13 (2) 443–460

Energy*Solutions*, 2020. *Radioactive Material Licenses UT 2300249 Cover Test Cell Deconstruction Study Final Report,* CD20-0123, Energy*Solutions* LLC, Salt Lake City UT, August 2020

Energy*Solutions*, 2021a. *Aggregate Gradation Form and Description and Identification of Soil (Visual-Manual) Worksheet,* CL-QC-PR-002-F7 and CL-QC-PR-002-F8, Rev. 1, Energy*Solutions* LLC, Clive UT, February 2021

Energy*Solutions*, 2021b. *Engineering Drawings, 14004-series Federal Cell Drawings (14004 U01, 14004 U02, 14004 U03, 14004 C01, 14004 C02, 14004 C03, 14004 C04, 14004 C05, 14004 Sketch 1),* Energy*Solutions* Clive Facility, Clive UT, June 2021

EPA, 2011. *Fact Sheet on Evapotranspiration Cover Systems for Waste Containment,* EPA 542-F-11-001, United States Environmental Protection Agency, Washington DC, February 2011

Fowler, H.J., et al., 2007. Linking Climate Change Modelling to Impacts Studies: Recent Advances in Downscaling Techniques for Hydrological Modelling, *International Journal of Climatology* 27 (12) 1547–1578 doi: 10.1002/joc.1556

Kennedy, W.E., et al., 1985. Biotic Transport of Radionuclides from a Low-level Radioactive Waste Site, *Health Physics,* 49 (1) 11–24

Maraun, D., 2013. Bias Correction, Quantile Mapping, and Downscaling: Revisiting the Inflation Issue, *Journal of Climate* 26 (2013) 2137–2143 doi: 10.1175/JCLI-D-12-00821.1

Maraun, D., et al., 2017. Towards Process-Informed Bias Correction of Climate Change Simulations, *Nature Climate Change* 7 (11) 764–773 doi: 10.1038/nclimate3418

Maraun, D., et al., 2010. Precipitation Downscaling Under Climate Change: Recent Developments to Bridge the Gap Between Dynamical Models and the End User, *Reviews of Geophysics* 48 (3) 1–34

MWH Americas, 2007. *Infilitration and Contaminant Transport Modeling Report, White Mesa Mill Site, Blanding, Utah,* prepared for Denison Mines (USA) Corp., MWH Americas Inc., Salt Lake City UT, November 2007

Neptune, 2005. *Mammal Parameter Specifications for the Area 5 and Area 3 RWMS Models,* Neptune and Company Inc., Los Alamos NM, September 2005

Neptune, 2015. *Neptune Field Studies, December, 2014, Eolian Depositional History Clive Disposal Site,* NAC-0044_R0, Neptune and Company Inc., Los Alamos NM, March 2015

Neptune, 2021a. *Biologically Induced Transport Modeling for the Clive DU PA, Clive DU PA Model v2.0,* NAC-0022_R3, Neptune and Company Inc., Los Alamos NM, September 2021

Neptune, 2021b. *Unsaturated Zone Modeling for the Clive DU PA, Clive DU PA Model v2.0,* NAC-0015_R5, prepared for Energy*Solutions*, Neptune and Company Inc., Los Alamos NM, September 2021

Neptune, 2021c. *Final Report for the Clive DU PA Model, Clive DU PA Model v2.0,* NAC-0024_R5, Neptune and Company Inc., Los Alamos NM, October 2021

Neptune, 2021d. *Deep Time Assessment for the Clive DU PA, Deep Time Assessment for the Clive DU PA Model v2.0,* NAC-0032_R6, Neptune and Company Inc., Los Alamos NM, August 2021

Neuman, S.P., et al., 2003. *A Comprehensive Strategy of Hydrogeologic Modeling and Uncertainty Analysis for Nuclear Facilities and Sites,* NUREG/CR-6805, United States Nuclear Regulatory Commission, Washington DC, July 2003

Rödenbeck, C., et al., 2001. Dynamical Systems with Time Scale Separation: Averaging, Stochastic Modelling, and Central Limit Theorems, *Progress in Probability* 49 (2001) 189–190

Rummukainen, M., 2010. State-of-the-Art with Regional Climate Models, *WIREs Clim Change* 1 (January/February 2010) 82–96

Scanlon, B.R., 1994. Water and Heat Fluxes in Desert Soils, 1. Field Studies, *Water Resources Research* 30 (3) 709–719

Scanlon, B.R., et al., 2003. Variations in Flow and Transport in Thick Desert Vadose Zones in Response to Paleoclimatic Forcing (0–90 kyr): Field Measurements, Modeling, and Uncertainties, *Water Resources Research* 39 (7) 1179 doi: 10.1029/2002WR001604

Scanlon, B.R., and P.C.D. Milly, 1994. Water and Heat Fluxes in Desert Soils, 2. Numerical Simulations, *Water Resources Research* 30 (3) 721–733

Schmidt, H., and A. Karnieli, 2000. Remote Sensing of the Seasonal Variability of Vegetation in a Semi-Arid Environment, *Journal of Arid Environments* 45 (2000) 43–59 doi: 10.1006/jare.1999.0607

Schwinning, S., and O.E. Sala, 2004. Hierarchy of Responses to Resource Pulses in Arid and Semi-Arid Ecosystems, *Oecologia* 141 (2004) 211–220 doi: 10.1007/s00442-004-1520-8

Šimůnek, J., et al., 2007. *HYDRUS (2D/3D), Software Package for Simulating the Two- and Three-Dimensional Movement of Water, Heat, and Multiple Solutes in Variably-Saturated Media, User Manual Version 1.0,* PC-Progress, Prague, Czech Republic, January 2007

Šimůnek, J., et al., 2005. *The HYDRUS-1D Software Package for Simulating the One-Dimensional Movement of Water, Heat, and Multiple Solutes in Variably-Saturated Media, Version 3.0,* University of California Riverside, Riverside CA, April 2005

Smesrud, J.K., and J.S. Selker, 2001. Effect of Soil-Particle Size Contrast on Capillary Barrier Performance, *Journal of Geotechnical and Geoenvironmental Engineering* 127 (10) 885–888

Smith, R.E., et al., 2002. *Infiltration Theory for Hydrologic Applications, Water Resources Monograph 15*, American Geophysical Union, Washington DC

Stephens, D.B., 1996. *Vadose Zone Hydrology*, CRC Press Inc., Boca Raton FL

SWCA, 2011. *Field Sampling of Biotic Turbation of Soils at the Clive Site, Tooele County, Utah,* prepared for Energy*Solutions*, SWCA Environmental Consultants, Salt Lake City UT, January 2011

SWCA, 2012. *Vegetated Cover System for the EnergySolutions Clive Site: Literature Review, Evaluation of Existing Data, and Field Studies Summary Report,* prepared for Energy*Solutions*, SWCA Environmental Consultants, Salt Lake City UT, August 2012

Teutschbein, C., and J. Siebert, 2012. Bias Correction of Regional Climate Model Simulations for Hydrological Climate-Change Impact Studies: Review and Evaluation of Different Methods, *Journal of Hydrology* 456–457 (2012) 12–29

Therrien, R., and E.A. Sudicky, 1996. Three-Dimensional Analysis of Variably-Saturated Flow and Solute Transport in Discretely-Fractured Porous Media, *Journal of Contaminant Hydrology* 23 (1–2) 1–44

Thompson, W.F., et al., 2015. *Stochastic Averaging of Dynamical Systems with Multiple Time Scales Forced with alpha-Stable Noise,* U. of British Columbia, Vancouver, BC, Canada, 2015

Tillman, F.D., et al., 2018. Effect of Spatial and Temporal Scale on Simulated Groundwater Recharge Investigations, *Advances in Water Resources* 119 (2018) 257–270 doi: 10.1016/j.advwatres.2018.07.014

Vogel, T., et al., 1991. Porous Media with Linearly Variable Hydraulic Properties, *Water Resources Research* 27 (10) 2735–2741

Wilby, R.L., and T.M.L. Wigley, 1997. Downscaling General Circulation Model Output: A Review of Methods and Limitations, *Progress in Physical Geography* 21 (4) 530–548 doi: 10.1177/030913339702100403

Wuebbles, D.J., and K. Hayhoe, 2004. Climate Change Projections for the United States Midwest, *Mitigation and Adaptation Strategies for Global Change* 9 (4) 335–363 doi: 10.1023/B:MITI.0000038843.73424.de

Yang, C., et al., 2017. Analysis of Temporal Variation and Scaling of Hydrological Variables Based on a Numerical Model of the Sagehen Creek Watershed, *Stochastic Environmental Research and Risk Assessment* doi: 10.1007/s00477-017-1421-0

Zhao, Y., et al., 2016. Modeling of Coupled Water and Heat Transfer in Freezing and Thawing Soils, Inner Mongolia, *Water* 8 (424) 1–18

References only available in hardcopy format will be provided separately. To access copies of these reference, please contact:

Division of Waste Management and Radiation Control
Utah Department of Environmental Quality
Multi Agency State Office Building
195 North 1950 West
Salt Lake City, UT 84116
Phone: (385) 536-0200

If you have further questions regarding the responses to the director's requests of DRC-2023-000537 for the Federal Cell Facility Radioactive Material License Application, please contact me at (801) 649-2000.

Sincerely,

Vern C. Rogers

Digitally signed by Vern C. Rogers
DN: cn=Vern C. Rogers, o=EnergySolutions, ou=Waste Management Division, email=vcrogers@energysolutions.com, c=US
Date: 2023.10.10 11:55:07 -06'00'

Vern C. Rogers
Director, Regulatory Affairs

enclosure

I certify under penalty of law that this document and all attachments were prepared under my direction or supervision in accordance with a system designed to assure that qualified personnel properly gather and evaluate the information submitted. Based on my inquiry of the person or persons who manage the system, or those persons directly responsible for gathering the information, the information submitted is, to the best of my knowledge and belief, true, accurate, and complete. I am aware that there are significant penalties for submitting false information, including the possibility of fine and imprisonment for knowing violations.